ArcGIS Inventory Analysis for Risk Assessment of Road Tunnels

By:

Simon Law

September 2023

Department of Civil Engineering

McGill University

Montreal, QC, Canada

A thesis submitted to McGill University in partial fulfillment of the requirements for the degree of Master of Science

This page is intentionally left blank

Acknowledgements

First, I express my sincere gratitude to Prof. Tim Xie, whose initial plans for this project and reliable consult throughout the project were essential for the successful completion of this thesis. Thank you for pushing me to challenge assumptions, require quality, and encouraging me to produce my best work.

In addition, I owe a deep debt to the community of scholars in the HMIR Lab at McGill University, especially Han Lin and Farzaneh Abedini, whose collaboration on elements of this research kept me on track and allowed me to move efficiently through trying times in the development of the end product.

Thank you to Stephan Lajeunesse and Pierre Gerdy Altidor of STM for their wisdom and collaboration in bringing elements of this project to work; indeed, thank you also to the expert knowledge of Audrey Beaudoin of FNX Innovation for soil data verification.

Finally, I owe a sincere thanks to my loved ones. To my parents, Kate and Adam, thank you for pushing me to demand the highest standard when pursuing my academic ambitions. To my siblings, Trevor and Julia, thank you for relieving the constant stress of research work with much-needed fun time. And lastly, to my girlfriend Chantel, thank you for your constant love and commitment in helping me push through the hard moments in this process.

Abstract

Tunnelling has been used for decades as a method for additional capacity in the transportation network. In recent decades increased interest in sustainable land usage and increasing space constraints have led many cities to replace urban freeways with underground sections. Risk analysis is a key issue for tunnels with high volumes of passenger car traffic due to occupancy and high-consequence accident scenarios. This thesis seeks to develop an inventory analysis system using ArcGIS to catalogue and use basic engineering data inputs to develop risk case studies for road tunnels. The basic framework of geospatial data referencing allows the user to develop a custom risk case scenario and add additional inputs to simulate relative risks and risk sensitivity to particular design factors, like tunnel depth or proximity to nearest egress.

A common risk scenario for road tunnels is confined fires. These are analyzed in a case study demonstrating the application of the ArcGIS inventory system to quantify fire risk components and risk response to design alterations. The system developed in ArcGIS maps the highest traffic volume roadways in Montreal if they were to be buried below their existing right of ways to reclaim land for sustainable development. The highest traffic route, the 'Metropolitan' highway 15 between Anjou and Decarie, is the subject of the case study evaluating the particular risk of fire due to the peak traffic loads, firefighting response time, and tunnel geometry for each point along the tunnel's length. By cataloguing the constituent risk levels for these factors in a rank-order matrix, this case study maps the relative risk levels for sampling points at a frequency of 100m, indicating the highest risk elements along the proposed tunnel network which could subsequently be addressed. Thereafter, a new fire station is theoretically placed to demonstrate the ability of this system to make risk-mitigating decisions with simple data analysis, which consequently lowers the peak nominal risk score from 100 to 60 at the highest risk tunnel position. Such, this framework is found to be potentially impactful in allowing industry professionals to process risk-based factors to analyze high-sensitivity sites in an existing or proposed tunnel network.

Rèsumè

La construction des tunnels est utilisée depuis des décennies pour augmenter la capacité du réseau de transport. Au cours des dernières décennies, l'intérêt accru pour l'utilisation durable des terres et les contraintes d'espace croissantes ont inspiré de nombreuses villes à remplacer leurs autoroutes urbaines par des sections souterraines. L'analyse des risques est plus important pour les tunnels plupart occupées par des voitures particulières en raison des scénarios d'occupation et des accidents aux grandes conséquences. Cette thèse vise à développer un système d'inventaire utilisant ArcGIS pour cataloguer et utiliser les entrées de données d'ingénierie tout simples pour développer des études de risque pour les tunnels routiers. Le cadre de base du référencement des données géospatiales permet à l'utilisateur de développer un scénario de risque personnalisé et d'ajouter des entrées supplémentaires pour simuler les risques relatifs et la sensibilité au risque à des facteurs de conception particuliers, comme la profondeur du tunnel ou la proximité de la sortie la plus proche.

Un scénario de risque courant pour les tunnels routiers est des incendies confinés. Ceux-ci sont analysés dans une étude de cas démontrant l'application du système d'inventaire ArcGIS pour quantifier les composants de risque d'incendie et la réponse au risque aux modifications de conception. Le système développé dans ArcGIS cartographie les routes les plus fréquentées à Montréal si elles devaient être enfouies sous leurs emprises existantes pour récupérer des terres à des fins de développement durable. L'itinéraire le plus fréquenté, l'autoroute 15 « Métropolitaine » entre Anjou et Décarie, fait l'objet de l'étude de cas évaluant le risque particulier d'incendie dû aux pointes de trafic, au temps d'intervention des pompiers et à la géométrie du tunnel pour chaque chainage du tunnel. En cataloguant les niveaux de risque constitutifs de ces facteurs dans une matrice de classement, cette étude de cas cartographie les niveaux de risque relatifs pour des points d'échantillonnage à une fréquence de 100 m, indiquant les éléments de risque les plus élevés le long du réseau de tunnels proposé qui pourraient ensuite être traités. Par la suite, une nouvelle caserne de pompiers est théoriquement placée pour démontrer la capacité de ce système à prendre des décisions d'atténuation des risques avec une simple analyse des données, ce qui réduit par conséquence le score de risque maximum de 100 à 60 à la position du tunnel à plus haut risque. Ainsi, ce cadre s'avère avoir un impact potentiel en permettant aux professionnels de l'industrie de traiter les facteurs basés sur les risques pour analyser les sites à haute sensibilité dans un réseau de tunnels existant ou proposé.

Table of Contents

List of Tables

List of Figures

Chapter I: Introduction

1.1 Introduction

Rapid urbanization in recent decades has seen quick rises in the demand for tunnel infrastructure to supplement the existing surface transit network. With substantial new construction and the ageing of 1960-era tunnels for both road and rail, there is a growing need and interest to monitor and simulate the behaviors of existing tunnels to inform risk-based decision-making in both practice and research. To incorporate sustainability, resilience, and durability considerations into both the construction of new projects and the monitoring and rehabilitation of existing infrastructure, developing new schemes to make efficient, risk-targeted decisions is necessary.

Given the increasing pressure to construct environmentally sustainable infrastructure in the 21st century, many cities have decided to explore the possibilities of transforming the operating mechanisms of their urban fabrics. At the forefront of this transformation is the decision to remove, replace, or bury their urban freeways [1].

For the city of Montreal, one predominant proposal is to remove the ageing autoroute-15 expressway and replace it with a subsurface road tunnel [2]. As early as 1989, replacing the ageing "Met" highway (autoroute 15) in Montreal with a tunnel was discussed [3]. The benefits of such a project include reducing carbon monoxide emissions, reducing traffic congestion, and improving the livability of the surrounding areas [1]. The precedents for burying highways in urban areas are not rare. As the most notable example, the city of Boston conducted a multi-billion, multi-decade project to bury a massive 10-lane multi-deck expressway and reclaim this wasted land as greenspace and urban amenity space [4]. This project has transformed the city character and its traffic performance. Dubbed the "big dig", this controversial project now saves the city upwards

of $500 million per year in maintenance costs and improves the traffic and livability of the city of Boston [4].

Freeway burial has been criticized as disastrous for traffic in increasingly gridlocked urban environments and a waste of taxpayer money. However, yesteryear's car-centric city planning ethos is now falling out of favour with a new generation who are increasingly concerned about their environmental footprint, health, and the livability of their cities. Moreover, even decreasing the total carrying capacity of a road artery, for example, by replacing an 8-lane highway with a 6-lane tunnel, generally has little to no effect on commute times, as those drivers deterred by the now-narrower, underground road would likely choose alternative means for their commutes - by switching to work-from-home, taking public transit, or using active transportation [5]. Influencing commuter behaviour through such “car-unfriendly” infrastructure projects, although controversial, doubtless would bear benefits for the entire population [5].

Nevertheless, tunnelling major urban auto infrastructure can increase its vulnerability to natural and man-made hazards such as fire, earthquake, and flooding. Despite the significant consequences, the risks of these hazards for urban highway tunnels have seldom been investigated. The objective of this thesis is to develop a systematic approach to streamline the processing of data inventory and develop a risk-based decision-making framework for planning and designing tunnel infrastructure. The major autoroutes in the urban core of Montreal are utilized as candidates for being replaced by tunnels, and the corresponding conceptual tunnel network is substantiated through an inventory analysis. Then, a case study is performed to assess the fire risk of the tunnel system.

1.2 Research Motivation and Objectives

This research is motivated by streamlining the sequencing of data information leading to an inventory database to facilitate infrastructure digitalization, automated tunnel design and construction, and risk-informed decision-making for risk mitigation. In particular, the work aims to directly utilize tunnel input parameters, such as geometry, geology, and code-complaint design constraints, to assess the fire-imposed tunnel risk and identify effective measures for risk mitigation. An ArcGIS database is developed for inventory analysis and risk assessment of the tunnel network, enabling the end user to visualize the system and pinpoint the high-risk components/locations within the network. The ArcGIS inventory also presents all data layers that can be used to develop high-fidelity finite element analysis for simulating tunnel behaviours and assessing the tunnel risk in a higher resolution. However, this work is outside the scope of the thesis but is part of the ongoing work of the HMIR Lab at McGill University. The inventory analysis and simplified risk assessment elaborated here serve as proof-of-concept for the ongoing work in the lab.

1.3 Organization of Thesis

The thesis first introduces the concepts of quantitative risk analysis and risk-based decision making, and reviews existing literature that explores these concepts using inventory analysis approaches. Then, key hazards relevant to the design of new-construction road tunnels are discussed. The thesis also discusses the context information relevant to the tunnel design and construction in Montreal. In the third chapter, prior literature is reviewed in more detail to identify existinf methods and research gaps pertaining to fires in road tunnels, to be used for a case study. The fourth chapter of the thesis covers the methodology of the inventory database developed for risk-based decision making in ArcGIS.

The fifth chapter of the thesis introduces design variables and a proposed method to quantify fire risk in road tunnels. This framework is then employed in a case study to assess the fire risk of the Montreal road tunnel network and recommend interventions to reduce hazard risk using the newly developed inventory tool. The limitations of the approach used in the case study and potential future work are discussed in the last chapter to conclude the thesis.

Chapter II: Background on Road Tunnel Replacement

This chapter surveys previous projects that explore the promise to replace road arteries with underground tunnels.

In North America and abroad, personal vehicles have been dominantly used for commuting. At the same time, worsening traffic and lengthening commute times urge many to believe there is a need for more road infrastructure. However, the opposite is true; replacing roadways with other modes of transit is proven to reduce road traffic for those who drive and improve the quality of commuting for those who do not [6].

At the leading edge of urban highway removal or burial is the new urbanist concept of induced demand. Namely, increasing the supply of roadways for vehicles thus induces a demand to drive, as this becomes the dominant and most accessible means of transport [6]. However, increases in road capacity are quickly overcome by more cars on the roads, often creating worse traffic than existed prior to any intervention [7]. The long-run induced demand correlation of new road infrastructure, bi-directionally, is almost exactly 1.0; hence, whether road capacities are increased or decreased, there is little to no impact on traffic and commuters over the long term, particularly if alternative transit modes are developed [8].

As reported by the Center for New Urbanism (CNU) [1], cities have compelling reasons to offer alternatives to urban freeways when their replacements come due. Urban freeways, especially those congested with slow-moving commuter traffic at rush hour, create a local hotbed of pollution and noise that have a severe dampening effect on property values nearby. As such, replacing urban freeways with alternatives, including boulevards, mass transit, or tunnels, not only saves municipalities millions in long-term maintenance, but also increases the property values in the immediate areas disproportionately. For instance, the CNU indicates that San Francisco’s

Embarcadero redevelopment project created a nearly 300 percent increase in property values and catalyzed development in a previously problematic region in less than a decade [1].

Many successful freeway removal or replacement projects have been completed in the last two decades, with the most representative one being the Boston “Big Dig” project. This massive project replaced the city’s deteriorating 6-lane urban expressway, analogous to Montreal’s autoroute 15 “Met”, with an underground expressway and replaced/expanded surrounding critical infrastructure, including two bridges and four new interchanges [9]. The dramatic transformation is shown between Figure 1 and Figure 2 [10]. This landmark project, which spanned 15 years, boasts a reported USD 168 million per year in savings due to decreased fuel consumption, lower accident rates, and a 62 percent reduction in traffic congestion through Boston’s downtown core between 1995 and 2003 [9]. Such significant improvements in road network performance come in tandem with the reclamation of the land used by the urban expressway into parks, public infrastructure, and other urban amenities. Despite its enormous upfront costs, the project shows proven benefits worth the investment.

Figure 1: Boston Central Artery (Before) [10] [11].

Figure 2: Boston Central Artery (After) [10] [11].

Chapter III: Literature Review

3.1 ArcGIS for Risk Assessment

ArcGIS is a raster-based geographical data management system used broadly to plan infrastructure, understand geotechnical site constraints, and manage data inventory for large projects. Previously, Khalil (2013), Shah et al. (2017), Griffin and Lixin (2021), and Wang (2021), have used ArcGIS to process geospatial data and develop a quantitative parameter risk analysis for road infrastructure and other civil engineering structures.

Suites of tools allowing the user to manipulate, interpolate, and investigate geospatial input data are the key functions in ArcGIS applicable to risk analysis. Khalil (2013) used ArcGIS Spatial Analyst to measure the proximity to natural hazards and quantify the relative risk of different options to place tunnel portals for a new highway in Saudi Arabia [12]. By quantifying the maximum proximity to (1) existing roadways, (2) mountains with minimum grades exceeding 6%, and (3) bodies of water requiring bridge crossings, their study produced a risk map displaying the suitable and unsuitable locations for the proposed roadway.

In their 2017 study, Shah et. al use GIS data to develop a neural-network-based iterative solution approach to produce an inventory risk-analysis for high-risk motorways in Belgium [13]. Vehicle speed, congestion, volume, and frequency across 67 segments of road on 2 highways in the province of Limburg were recorded as 4 input parameters. Artificial neural networks were then used to simulate the risk by mapping the risk outcome levels (e.g. number of fatal car crashes in a time period) relative to input parameters (e.g. average traffic congestion over the same period), where interventions were recommended to further maximize the road safety [13]. One essential step of this process is to identify the risky road segments at peak input intensities. This step is achieved using GIS to rank road segments according to all data elements, where the risk of each

road segment is calculated as the weighted sum of all risk outputs divided by the weighted sum of input parameters [13]. This approach can be adapted to conduct a straightforward GIS analysis of risk with known inputs, controlling for data weights at the user's discretion.

GIS is also a useful tool to store records of data in order to observe existing trends and make evidence-based policy interventions. In the example of Lixin and Griffin (2021), records of car crashes from 2010 – 2015 on highways in Brevard County, Florida, were geospatially logged to understand the highest risk positions on the network [14]. In this study, the Euclidean distance of crash locations and crash outcomes were recorded within ArcGIS, and a statistical regression was performed to identify crash "hot spots" along the highway network. As such, aggregating and presenting the data in GIS allowed the authors to pinpoint periods and locations where critical collisions were most likely to happen. The ArcGIS also allows these findings to be presented graphically and communicated to the transit commission for recommending effective interventions [14]. The approach to identifying high-risk infrastructure ArcGIS is of key consideration when using inventory analysis to make informed design decisions.

Wang (2021) used ArcGIS to develop a quantitative risk assessment map by summing constituent risk elements and mapping them according to four hazard levels, namely low, moderate, high, and very high. This study uses Equation 1 below to obtain the risk level at each position:

$$R(i) = \sum_{i=1}^{n} H(i) * C(i)$$

Equation 1: Element Risk Quantity

here R(i) is the risk score of the ith element under investigation, H(i) refers to the risk level of the element, and C(i) is the consequence of the particular hazard under investigation [15].

3.2 Risk Assessment of Underground Infrastructure

Prominent hazards for underground transit tunnels include fire, flood, and earthquake. The fire hazard is most relevant to road tunnels, as is the focus of this research. Risk analysis of road tunnels involves designing specific segments of roads and evaluating their risks independently and probabilistically, where the highest-risk segments are prioritized for mitigation strategies. For example, Schubert et al. considered the generic segmentation of a fictitious road system and used this concept through a Bayesian network for risk analysis under a design fire scenario of a high-flammable heavy truck [16].

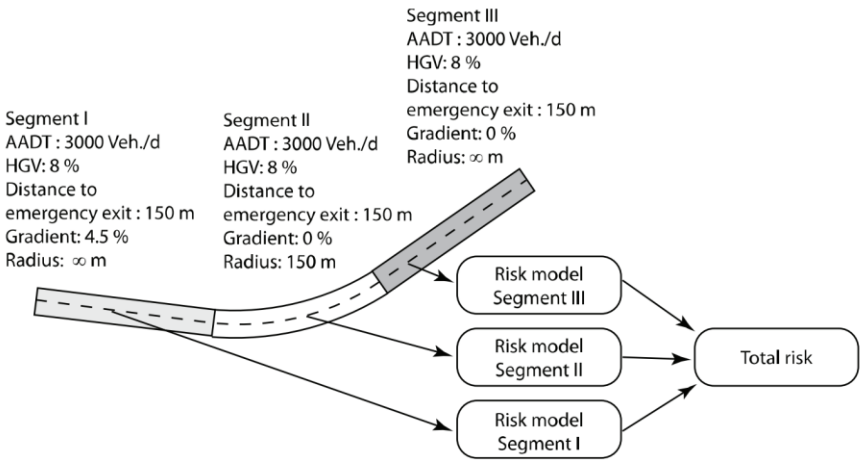

Figure 3: Segmentation for Constituent Risk Analysis, Bayesian (from Schubert et al.) [16]

Herein, risk metrics are commonly computed as the product of the consequence and the probability of damage under each design outcome [17]. Combining the utility of GIS and the features of risk analysis is a core component of this thesis. The work from Thaker and Savaliya (2018) introduces the mapping of seismic risk in Ahmedabad, India, by conducting a multi-criteria analysis (MCA) [18]. A hierarchical process that identifies the priority of design risk factors and weighs them relative to each other in a pairwise comparison matrix is used within this study to score the level of seismic risk on a geospatial basis [18]. The weighted sums are then compared to benchmark

values along a spectrum for each parameter to assess the influence of each value on the risk at a given point. As such, a risk map can be produced to show the overall risk score of each point in a system.

The direct study of natural hazard risk using GIS to analyze effects on a transportation network is not well studied but has been considered by Danila et al. (2020) for the region of Bucharest, Romania [19]. This study defined a methodology for modelling the vulnerability to natural hazard of key infrastructure (bridges, tunnels), and measuring post-disaster response, with the target of measuring probability of network failure due to natural hazards. Monte Carlo simulations were used to concurrently simulate multiple-scenario risk, and the data was analyzed and displayed within ArcGIS using the Network Risk toolbox, which was restricted for use in this study [19]. Applying network risk analysis, this study concluded that the excess risk due to seismic activity was highest on the south-eastern region of the city of Bucharest, and recommended the strategic placement of a new hospital in this region to retain access to healthcare during an emergency scenario [19].

3.3 Design Factors Influencing Fire Risk

Design factors need to be considered to reduce the occurrence and severity of fire events in road tunnels. ISO fire guidelines recommend structural integrity be maintained for a minimum of 60 minutes and 120 minutes for a tunnel in unstable soil and rock or well-founded soil, respectively [20]. Beyond this constraint, tunnel performance in fire scenarios must also be considered to minimize fatality and economic losses, where the egress and air circulation should be designed based on the required minimum performance metric [21].

The direct fire risk to structures is secondary to the fire safety in a road tunnel, given its occupancy and throughput within a confined area. As such, designing egress points to ensure that affected

persons in the fire event could flee on foot within 30 minutes as well as designing a minimum CFM air circulation to move smoke from a fire event would minimize the likelihood of death and destruction. These concepts are well documented in the review of Road Tunnel Fire Safety by Gehandler [21], which will be discussed in the case study later in this thesis.

Chapter IV: Inventory Analysis of the Road Tunnel Network through ArcGIS

Compiling a dataset is the first step for conducting an inventory analysis through ArcGIS. The location of the proposed road tunnel network has been decided to replace Montreal's congested road arteries. Using data information from various sources, a comprehensive dataset is compiled to investigate the surrounding rock/soil conditions in Montreal island. Afterward, an ArcGIS map is developed and refined to compile the tunnel-soil/rock data information useful for the risk assessment. These steps are detailed in this section.

4.1 Montreal Island Geology

The long geological history of the island of Montreal is well chronicled in academic literature. A paper trail of borehole studies for both private and public-sector records that exist in the public domain chronicle the stratigraphy of soil layers, and essential geospatial assets can be determined using the ArcGIS world atlas. The Island of Montreal is situated within the Canadian Shield region, most of the rock of which is Paleozoic limestone and limestone schist, overlain by several layers of soft sedimentary shale rock and/or soils [22]. The rock forming the base and main extrusion of Mount Royal in the centre of the downtown region is the igneous rock formed by ancient volcanoes, whose magma chambers and deepest components now remain after hundreds of millions of years of erosion [23]. The gabbro of Mount Royal is restricted to that specific locale, with no other mountainous igneous outcroppings within the urban region of Montreal [22].

Bedrock occurs at a mean depth of 13 m across the island, with the North and Northeast regions containing only very shallow surface overburden and frequent outcroppings [24]. Soil penetrates much deeper on the southern exposure of the island, where repeated silt deposition from the St. Lawrence River has added granular material over millennia [25]. The STM Metro project, which comprised over 60km of track across several boroughs in Montreal and across the St. Lawrence

River, has bored tunnels in a variety of these subsurface strata, including trench construction in soft soils, blasting, and boring deep within bedrock (>25m) into solid rock [24].

The soil layers most prevalent on the southern side of the island of Montreal owe their presence to the repeated glaciation of the region and deposition of sediment by the St. Lawrence River system. The shallow soil layers that remain today comprise dense, sometimes wet sands, clays, and silty tills of high bearing capacity [25]. The two figures below display the surface geology (Figure 4) and the bedrock geology (Figure 5) across the island of Montreal [26] [25].

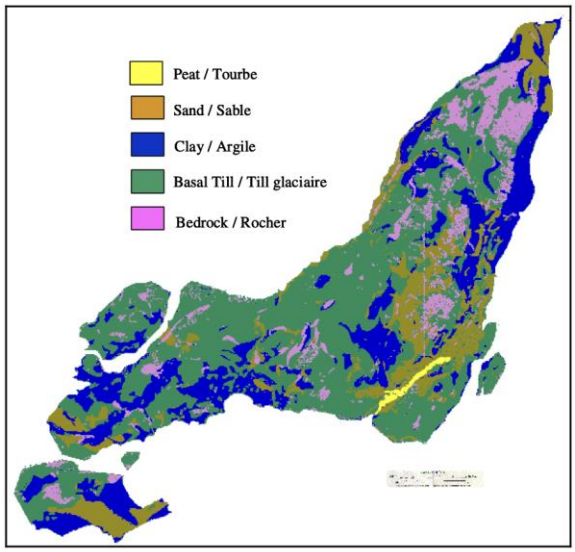

Figure 4: Surface Geology for Montreal Island [26]

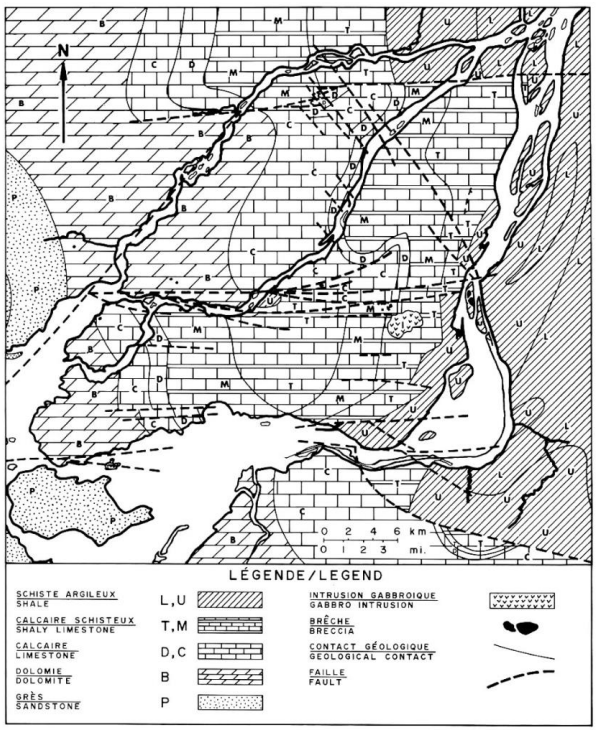

Figure 5: Bedrock Geology for Montreal Island [25]

4.2 Positioning the Tunnel Network

Montreal has multiple tunnels of various uses, including the STM Metro system, the Ville-Marie expressway underground section through downtown, and the Louis-Hippolyte-La Fontaine road tunnel providing a river crossing underneath St. Lawrence on Autoroute 25 [27]. In addition to

these tunnels, a new road tunnel network is proposed to improve urban air quality, liberate land use in the downtown core, and reduce traffic noise. As such, the positioning of the new tunnel needs to consider the following constraints:

- Road tunnel lines will be placed where their surface road counterparts currently exist.
- The road arteries for tunnel replacement are those with the highest peak traffic congestion.
- The total length of the tunnel will approximate 70 km, which is consistent with the tunnel length within the STM Metro network.
- The tunnel is designed to have 3 traffic lanes for each artery, with one lane for entries/exits at a reduced speed.

By taking into account the above constraints, mainly the traffic congestion map shown in Figure 6 [28], the road tunnel network is proposed and depicted in Figure 7.

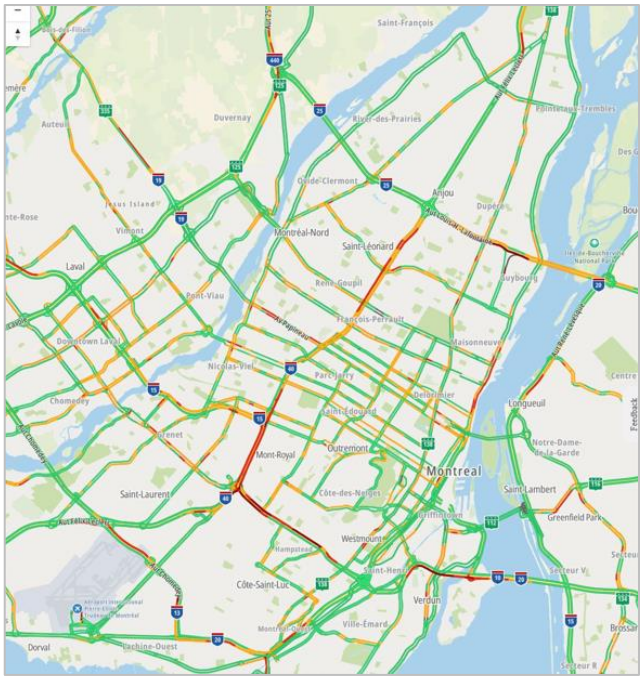

Figure 6: Montreal Traffic Congestion Map [28]

Figure 7: Tunnel Route Based on Traffic Mitigation

4.3 Assembling Soil Database

The risk of the tunnel network under different hazard scenarios also depends on its surrounding soil and rock conditions. Building upon previous studies, soil layers in Montreal can be classified into gravel, sand, silt, and clay, whereas soil properties for each soil type include the bulk unit weight, Young's modulus, friction angle, and Poisson ratio. The reference data and methodology for sourcing each property are detailed in this section. Although the soil layers in which tunnels are immersed are not a necessary design factor for all types of risk analyses, they form an essential component of the general-use design of the tunnel system.

Sourcing inventory data involves referencing the existing literature on geological information and construction documents available in the public domain to find quality data sets. To develop a useful framework for risk indexing, the tunnel depth, surface elevation, and soil layer depth at a reasonably high resolution were required at a minimum.

The primary source for the data set discussed hereafter is a database of borehole sheets from the original construction of the Montreal Metro system in the 1960s, which offers a high-resolution interpretation of the depth of soil layers around the island of Montreal. Estimated to the nearest foot and converted to meters for consistency, these values make up the primary data.

Statistics of the soil/rock profiles along the proposed tunnel network are presented in Table 1. The profile statistics summarize the distribution type, mean value (μ), standard deviation (σ), the parameter range with plus/minus two standard deviations, and the number of data points considered for each profile parameter, including surface elevation, thicknesses of gravel, sand, silt, and clay layers, rock depth, and track depth. The distribution fits of each parameter are further illustrated in Figure 8. As shown in the figure, statistical distribution matches the true frequency of the considered data for each parameter.

Table 1. Soil/Rock Tunnel Profile Statistics

Data	**Distribution**	**μ**	**σ**	**Range**	**Number of Data Points**
Surface Elevation	Normal	42.3	25.8	-10.7 – 129.5	2166
Track Depth	Normal	21.4	9.0	4.9 – 64.0	2023
Gravel Thickness	Lognormal	3.7	3.4	0 – 19.8	736
Sand Thickness	Lognormal	5.5	5.0	0 – 36.0	1511
Silt Thickness	Lognormal	7.5	7.1	0 – 38.2	769
Clay Thickness	Lognormal	8.5	7.1	0 – 38.2	360
Rock Depth	Lognormal	39.4	50.3	-10.7 – 152.4	1992

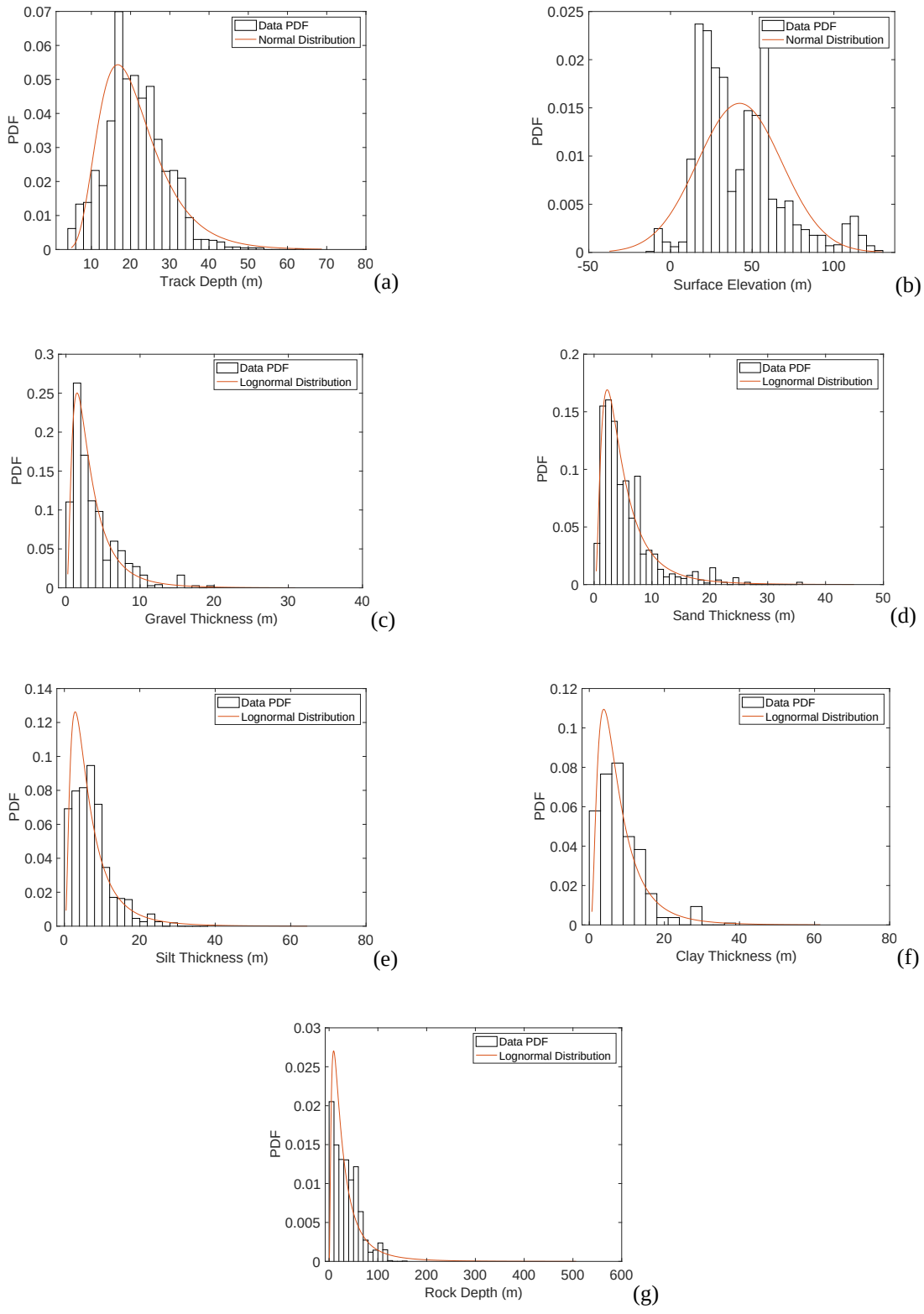

Figure 8. Histogram Trends for Tunnel Soil Data Sets

Geometry for the soil layers is the primary element making up the GIS Inventory used later to demonstrate risk analysis techniques in a case study. As part of the investigation of soil properties, an investigation of the soil property characteristics in Montreal was also done, as shown in Appendix I.

4.4 Inventory Data Analysis

A complete inventory detailing the position of geospatial assets for the proposed tunnel network had to be assembled to understand the relationship of the proposed tunnels to the existing street grid. This was achieved by assembling data from a broad range of public and private sources in an Excel table, using layer-ordering logic and data trimming to publish a refined data set for functional use in this study, and importing this information into a presentable format using ArcGIS Map tools.

The depth of tunnels is distributed based on typical tunnel burial depths for existing infrastructure in Montreal, as displayed in Figure 9, using reference information shared by the STM.

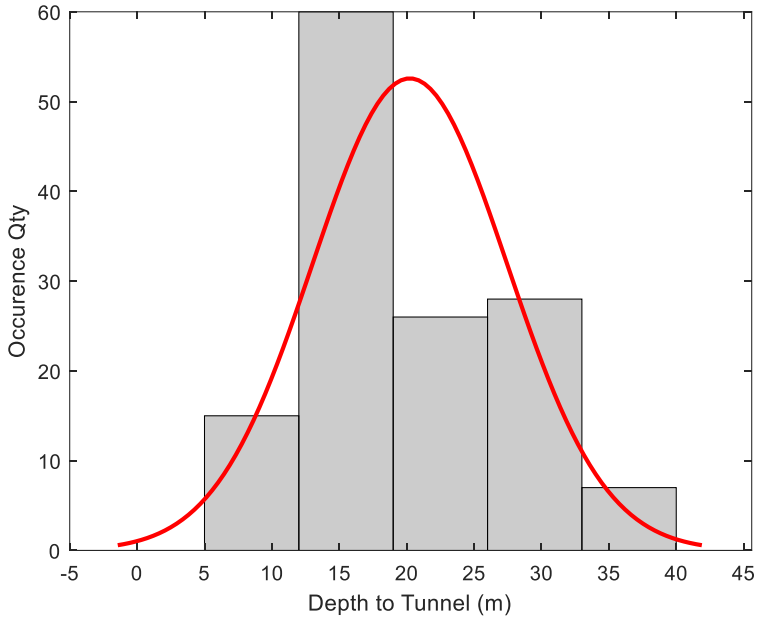

Figure 9: Tunnel Depth Statistical Trend and Histogram (Normal Regression)

Lastly, the surface elevation and position of the tunnel had to be denoted at a consistent resolution to provide local points to store the other data elements. This was completed directly in ArcGIS, where the surface elevation survey data was used to pinpoint surface elevation, and the XY geospatial reference data was recorded at 100m intervals along the lines of the theoretical road tunnel network, which corresponds to the position of the existing freeways. The nearest borehole reference was used for each point source for determining soil/rock profiles. Figure 10 shows how toggling a specific point in the ArcGIS map with the desired data level toggled will display a pop-up box giving the XY coordinates and the Z elevation relative to sea level [29]. NAD 1983 MTM 8 standards are used for the X and Y coordinate data, given in meters, throughout this study.

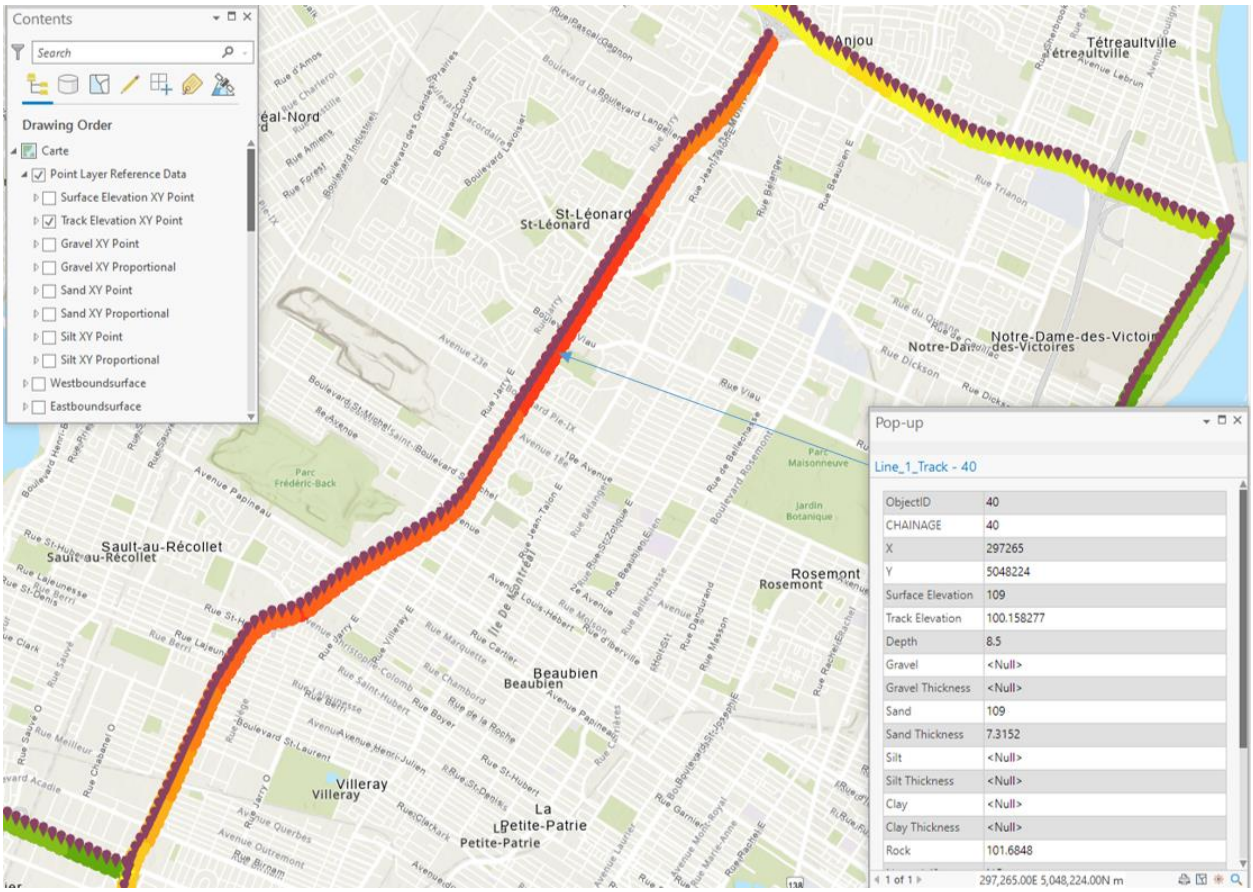

Figure 10: ArcGIS Project Window Showing Toggled Data Point Information Pop-Up

4.5 Processing Data in Microsoft Excel

Data was pre-processed in Microsoft Excel to create data tables and develop the feature layers in ArcGIS. This process began with disseminating layer depth information from borehole sheets into a value table and correlating boreholes to the nearest sampling point of the tunnel data every 100m. Generally, layer depth was recorded with an estimate to the nearest 0.5m, and soil layers are considered consistent with the local soil condition. For example, a given layer may only contain sand between the bedrock and the ground surface, where another location may have gravel over sand over silt. The first step in preparing the data set was adding the surface elevation and tunnel elevation information into the spreadsheet at intervals of each 100m, denoted as "sample points". Table 2 shows the database framework, with each sample point having a correspondent XY position, surface elevation, and tunnel elevation.

Table 2: Input Data I: XY and Tunnel Elevations

STATION	X	Y	Surface Elevation	Tunnel Floor Elevation	Depth
1	299483.00	5051432.00	107.54	88.82	17.37
2	299430.00	5051349.00	106.68	88.39	18.29
3	299379.00	5051265.00	106.39	88.37	19.51
4	299326.00	5051177.00	107.64	86.63	21.95
5	299276.00	5051084.00	108.20	84.62	24.38
6	299222.00	5051004.00	108.33	82.30	26.52
7	299163.00	5050923.00	109.50	80.77	28.96
8	299113.00	5050837.00	109.43	80.57	29.57
9	299053.00	5050759.00	111.25	80.75	30.78
10	298988.00	5050679.00	112.21	79.91	31.70
11	298917.00	5050610.00	112.31	79.55	32.92
12	298848.00	5050536.00	112.17	79.88	33.83
13	298771.00	5050472.00	114.00	80.66	33.83
14	298698.00	5050403.00	113.33	82.20	32.92
15	298626.00	5050332.00	114.68	83.52	30.78
16	298561.00	5050257.00	114.90	85.34	28.96
17	298503.00	5050175.00	114.89	87.28	27.13

18	298451.00	5050094.00	114.30	89.66	24.99
19	298393.00	5050008.00	114.84	91.83	22.86
20	298339.00	5049923.00	113.80	92.48	22.30

The soil layers were then added to complete the full ground profile at each sample point. Soil layer information was interpreted from the borehole reference sheets provided by the STM, as previously discussed in Section 4.3 By default, the master data table is configured to assume that the "typical" soil layer order from surface to rock is gravel above sand above silt above clay. On this basis, the layer thickness for each soil layer was determined by subtracting the elevation of the layer below it. Equation 2shows the formula that computes the layer thickness from the relative soil layers depths in Excel, with Table 3 showing a sample of soil position and thickness data for the same excerpt as Table 2.

```
=IF(AND(OR(D2-F2>0,D2-F2<0),OR(F2>0,F2<0),OR(D2>0,D2<0)),ABS(D2-F2),(IF(AND(OR(D2-H2>0,
D2-H2<0),OR(H2>0,H2<0),OR(D2>0,D2<0)),ABS(D2-H2),(IF(D2>J2,D2-J2,0)))))
```

Equation 2: Formula for Layer Thickness Computation

In Equation 2, the order of layers is checked, then the correct order for the given chainage is used to compute the layer thickness value for the given cell, as demonstrated for Sand Thickness at Station 1 in the sample calculation. Rows are labelled in Table 3 for reference.

Table 3: Input Data II: Soil Layer Information

STATION	Gravel Elevation	Gravel Thickness	Sand Elevation	Sand Thickness	Silt Elevation	Silt Thickness	Rock Elevation
1			105.00	1.68	106.68	4.85	101.83
2	106.68	1.24			105.46	6.10	99.36
3	106.98	1.81			105.17	5.50	99.67
4	107.59	1.21			106.38	6.10	100.28
5					107.57	17.18	90.39
6					109.58	17.70	91.88
7					109.73	17.37	92.35
8			110.65	2.18	108.46	5.33	103.13
9			111.25	0.52	110.73	6.88	103.85

10	111.70	0.41			111.29	16.80	94.49
11	112.08	1.53			110.56	15.46	95.10
12	113.08	1.13			111.95	4.97	106.98
13	114.00	0.91			113.08	5.18	107.90
14			113.71	0.63	113.08	0.98	112.10
15			114.30	1.27	113.03	1.78	111.25
16			114.89	2.36	112.52	0.62	111.90
17			114.84	1.39	113.45	2.33	111.12
18			114.01	1.54			112.47
19			114.74	2.03			112.72
20			113.80	20.20			93.60

Comparative logic statements were used throughout the table to make checks on the order of layers and display the correct layer thickness if a soil layer is either not present or not in the expected default order. This logic allows the inventory to evaluate the vertical order of soil layers and their respective depths within a soil profile. Soil layers not in the “typical” order – of gravel above sand above silt above clay - are distinguished by the check in Equation 3 of layer normalcy. This formula identifies each soil layer at a given station, and where the other typical soil layers occur relatively. Hence,

Table 4 labels each station as having a “Normal 4?”, “Normal 3?”, or otherwise soil profile based on if the typical order is followed and based on the number of soil types at that station. If any of these conditions are met, the program concludes that there is a “normal” soil profile at that station. For example, consider the profile at station 1, where Equation 3returns “YES” for the condition of “Normal 2?”, indicating that this profile has 2 layers of soil and meets the typical order constraint. Hence, station 1 has a normal soil profile. These results are summarized for the first 20 stations in Table 4.

```
=IF(OR(AND(G2>0,I2>0,K2>0,M2=0,G2>I2>K2),AND(G2>0,I2>0,M2>0,K2=0,G2>I2>M2),AND(G2>0,
K2>0,M2>0,I2=0,G2>K2>M2),AND(G2=0,I2>0,K2>0,M2>0,I2>K2>M2)),"YES","NO")
```

G2 = Gravel Layer I2 = Sand Layer K2 = Silt Layer M2 = Clay Layer

Equation 3: Layer Ordering Logic Equation for Station 2 with Legend

Table 4: Layer Order Checks for Stations 1-20, Corresponding to Table 4

STATION	Normal 4?	Normal 3?	Normal 2?	Normal 1?	Normal Rock?	Normal Layer?
1	NO	NO	YES	NO	NO	YES
2	NO	NO	YES	NO	NO	YES
3	NO	YES	NO	NO	NO	YES
4	NO	YES	NO	NO	NO	YES
5	NO	YES	NO	NO	NO	YES
6	NO	YES	NO	NO	NO	YES
7	NO	YES	NO	NO	NO	YES
8	NO	YES	NO	NO	NO	YES
9	NO	NO	NO	NO	NO	NO
10	NO	NO	NO	NO	NO	NO
11	NO	NO	NO	NO	NO	NO
12	NO	NO	NO	NO	NO	NO
13	NO	NO	NO	NO	NO	NO
14	NO	NO	NO	YES	NO	YES
15	NO	NO	NO	YES	NO	YES
16	NO	NO	NO	YES	NO	YES
17	NO	NO	NO	YES	NO	YES
18	NO	NO	NO	YES	NO	YES
19	NO	NO	NO	YES	NO	YES
20	NO	NO	NO	YES	NO	YES

Layer thickness and position are the primary characteristics to develop the qualitative soil profiles shown for the entire proposed network of tunnels in ArcGIS.

4.6 ArcGIS Tunnel Network Development

The organization of data into a prepared set in Excel was a precursor to developing a geospatial inventory map in ArcGIS. This section discusses how this data was developed in ArcGIS Pro to create an interactive feature map that can be used for risk analysis.

According to the above discussions, the tunnel network is positioned to cover the highest-congestion roadways subjected to tunnel replacement. This network comprises a total of 656 sample points at a 100 m interval for a total tunnel length of 65.6 km. ArcGIS Pro allows for thorough geographical exploration and asset management. To have a map that is useful for an end user to acquire geospatial information and to implement further information layers to display risk mapping and response results, tools within the geospatial analyst toolbox need to be used.

First, all data layers were added to the map using the “XY Table to point” function once all data tables had been imported from Excel directly into ArcGIS’s catalogue window. Henceforth, individual data layers can be manipulated using a particular symbology, prominence, and other functional tools. Figure 11 shows the basis map window in ArcGIS with the catalogue of point data and the tunnel depth points visible within the window.

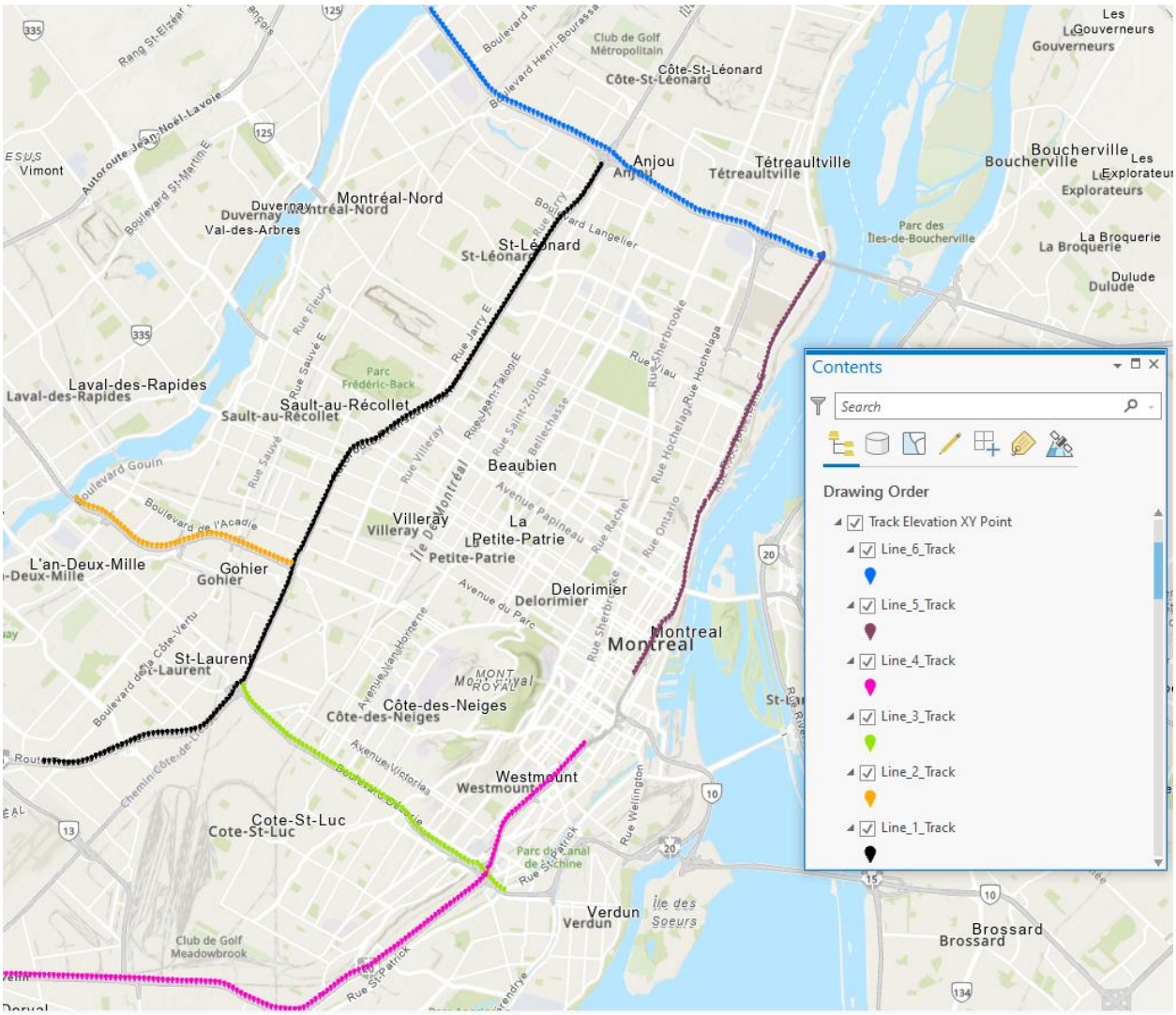

Figure 11: Point Layer Reference Data for Tunnel Track Depth

To develop the functionality desired for exploring the map and acquiring quantities at a desired point, raster layers were added to the map using inverse distance-weighted rastering with a 500 m elevation influence. These results create a smooth profile where an interpolated elevation for any data layer can be queried in the software. Figure 12 shows the raster layer for tunnel depth with an intermediate call-out point denoted with an arrow.

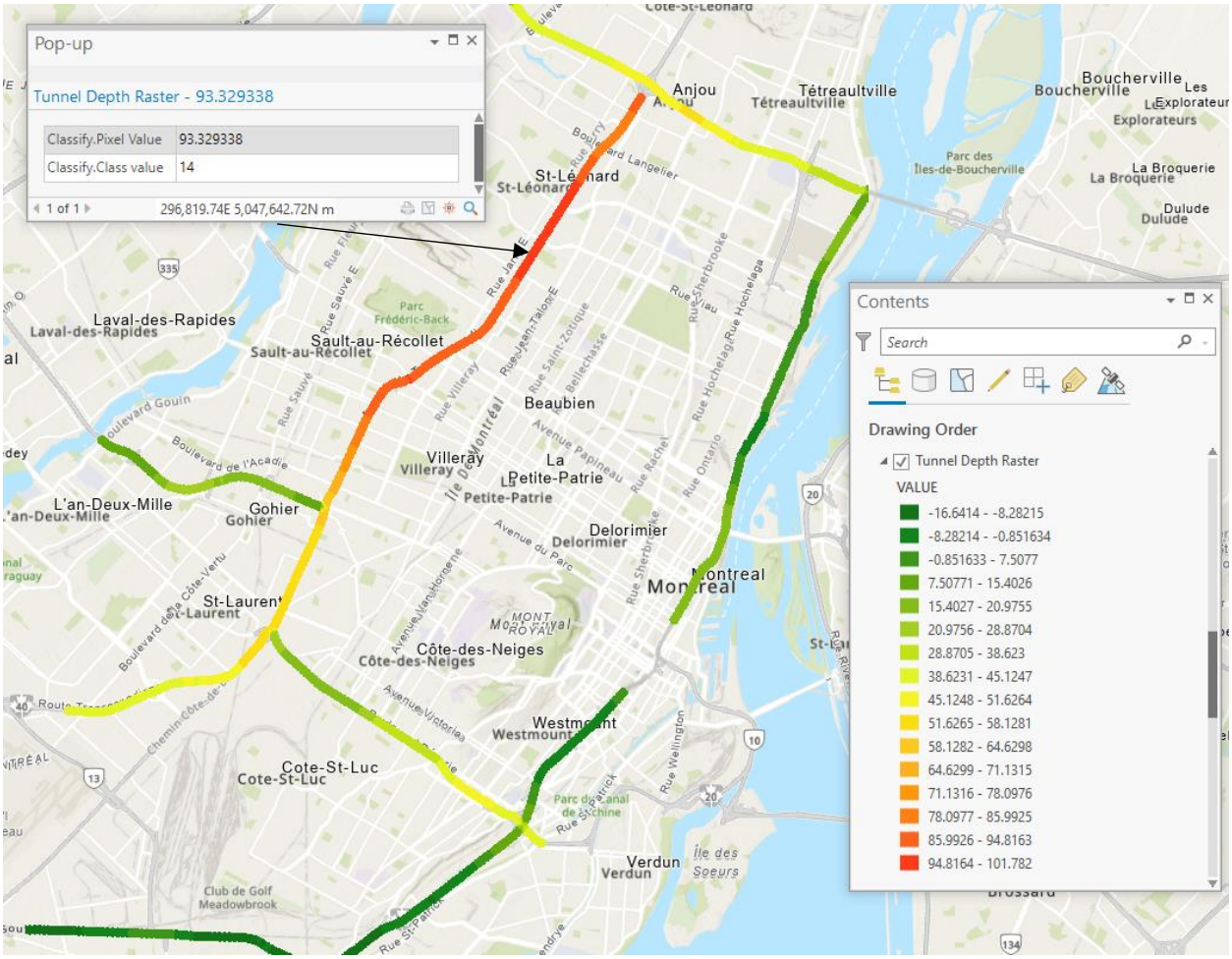

Figure 12: Raster of Tunnel Depth showing Pop-Up of select point

Finally, the ArcGIS map can be expanded to suit the needs and data requirements of any studies related to spatial analysis. For this project, the utility of the map will be demonstrated with a fire risk case study shown in the following section, where new data layers for fire station locations, emergency egress proximity, and traffic will be mapped to produce a composite risk index.

Chapter V: Fire Risk Assessment of the Road Tunnel

5.1 Case Study Scenario

To demonstrate the utility of the developed ArcGIS inventory system, the case study conducts risk assessment and mitigation of road tunnels against fire hazards. The Autoroute 40 between Anjou and Decarie (the "Metropolitain") is selected for this case study, as shown in Figure 13.

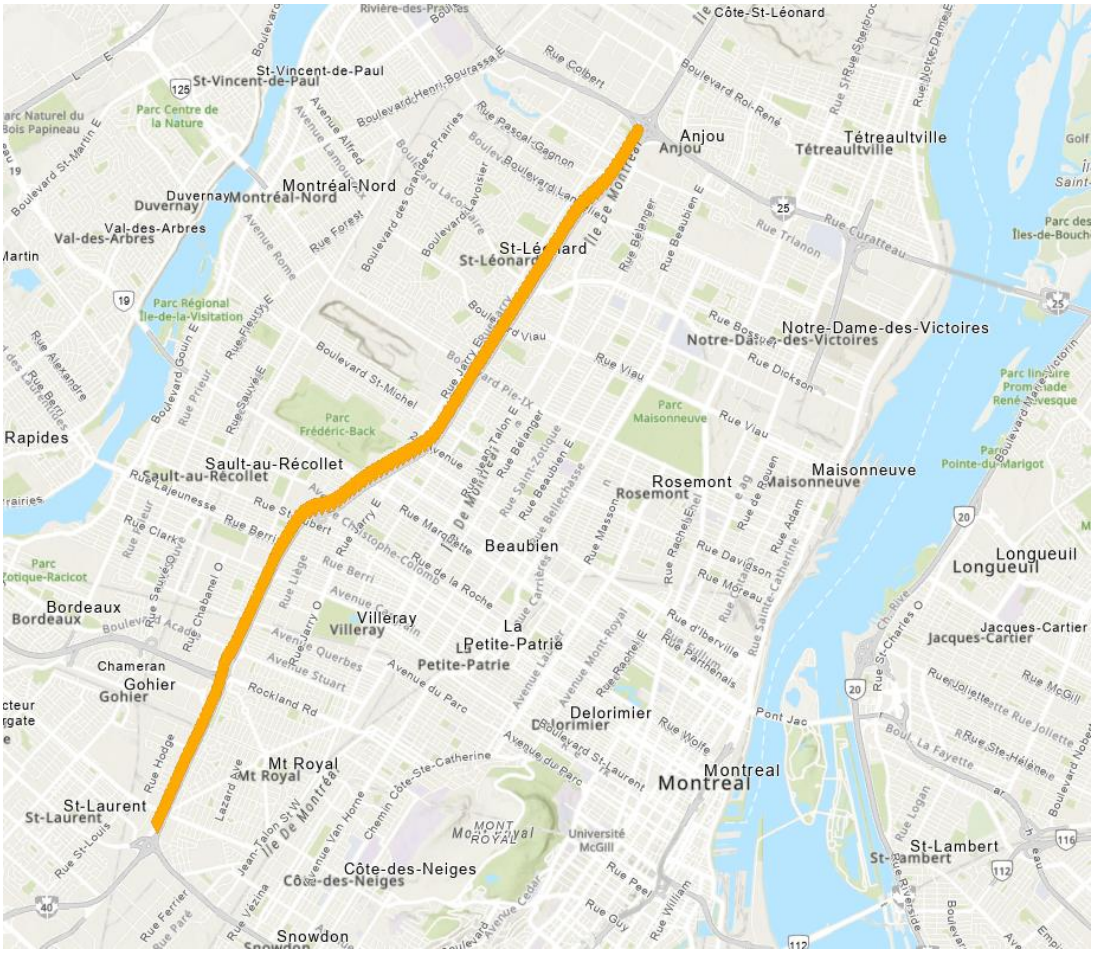

Figure 13: Map window showing case study segment

General Approach

The risk analysis considers influential factors during an uncontrolled fire event within a road tunnel. These factors include the distance to the nearest egress, fire size, traffic characteristics, and

accessibility of fire suppression infrastructure. Influences from these factors are statistically evaluated through a matrix based on the existing literature, producing a multi-variable risk function mapped along the tunnel line of interest. These input parameters are discussed first, with the development of the risk model to follow. The target output of this study is a dynamic, geospatially referenced risk output that can be used to explore the sensitivity of fire risk to various inputs.

Traffic Frequency, Design Speed, and Tunnel Entry/Exit Stations

The first input factor considers the throughput of vehicles through the designed road tunnel. Recent estimates of the traffic in the busiest section of Autoroute 40 in Montreal project a peak throughput of 177,000 vehicles per day [2]. Typically, 15% of the traffic on a highway route can be considered as large cargo or trucking traffic; however, since this highway route comprises the main bypass through the downtown core of Montreal and is on the Trans-Canada highway network with reports of a high amount of congestion from trucking traffic, the rate of cargo and trucking vehicles is set at 25%, or 44,250 vehicles per day [21]. These peak values are treated as the limit states that will cause traffic congestion. A second case scenario where trucks are diverted to a surface road and the tunnel is only permitted for cars is also considered. This case has a peak traffic load of 132,750 cars per day, and no trucks will be considered.

Traffic flow in a tunnel typically runs at a lower speed than on an elevated or at-grade highway. Therefore, a design traffic speed of 80 km/hour is considered here [30]. This also corresponds to the nominal design speed for emergency vehicles to respond to an accident site.

The next key variable to consider is the distance or frequency of egress points/exits for vehicles/people to leave the tunnel in an emergency scenario. Taking roadway exits as an example, approximately 16 entry/exit points have been designed for the same highway section spanning 14 km long. 11 entry/exit points are major interchanges, and 5 are used to merge lane entry points

from a feeder road. Hence, 11 egresses are considered for the equivalent tunnel segment. The schedule of on-ramp lengths for the 11 major egresses is shown in Table 5 assuming a 4% slope for connecting on and off ramps to the design depth of the tunnel.

Table 5 : Egress Paths Summary

EXIT NAME	ROAD DIRECTION	EXIT NUMBER	ENTRY POS X	ENTRY POS Y	TUNNEL ENTRY X	TUNNEL ENTRY Y	ENTRY PATH (m)
ANJOU	EASTBOUND	1	299469	5051373	299129	5050754	703.01
LANGELIER	EASTBOUND	2	298711	5050387	299276	5050996	852.56
LACORDAIRE	EASTBOUND	3	297902	5049142	298064	5049381	288.96
VIAU	EASTBOUND	4	297477	5048469	297670	5048769	355.45
PIE IX	EASTBOUND	5	297032	5047824	297292	5048196	453.37
ST MICIHEL	EASTBOUND	6	296503	5046935	296946	5047609	804.53
PAPINEAU	EASTBOUND	7	295341	5046034	296377	5046717	1257.6
ST LAURENT	EASTBOUND	8	293770	5044652	293993	5045034	432.32
ACADIE	EASTBOUND	9	293220	5043430	293390	5043735	347.32
TC15	EASTBOUND	10	292782	5043037	293111	5043250	408.25
DECARIE	EASTBOUND	11	291984	5040273	291922	5040514	241.00
ANJOU	WESTBOUND	1	299426	5051402	299026	5050803	733.15
LANGELIER	WESTBOUND	2	298640	5050431	298322	5049977	548.72
LACORDAIRE	WESTBOUND	3	297805	5049192	297682	5048989	236.97
VIAU	WESTBOUND	4	297400	5048525	297199	5048204	382.36
PIE IX	WESTBOUND	5	296990	5047847	296553	5047190	789.09
ST MICIHEL	WESTBOUND	6	296428	5046982	295739	5046335	917.04
PAPINEAU	WESTBOUND	7	295235	5046117	294450	5045587	937.40
ST LAURENT	WESTBOUND	8	293728	5044674	293395	5043938	816.37
ACADIE	WESTBOUND	9	293161	5043470	292910	5042904	612.22
TC15	WESTBOUND	10	292810	5043105	292793	5042582	500.00
DECARIE	WESTBOUND	11	291982	5040237	291891	5040529	292.00

Emergency Response Time and Egress

The tunnel needs to be escapable in a reasonable time frame and accessible for quick responses from emergency responders during a fire event. The two relevant variables are the distance to the nearby fire hall and the response-to-site time for a fire engine to arrive at the given fire site in the

tunnel. Based on the work of Merrell [31], 90% of calls deliver a first fire engine to the fire site within 240 seconds. However, for the risk assessment of this study, fire trucks are assumed to travel at the design-level traffic speed through the shortest roadway path from station to fire, with a 25% reduction to account for congestion. The response time will then be computed to develop a risk score.

As recommended by road tunnel designs, egress to a safe exit passageway should be considered at a minimum of every 300 m [32]. This is achieved by constructing a ventilation service tunnel adjacent to the traffic tunnel in each direction, with exit stairwells established at the midpoint of road exit points along the tunnel's length [32]. The proposed exit locations and road ramp locations are elaborated on in the next section, together with the risk to safe egress measured based on distance.

Fire Event Scenarios

The conditions for a fire event in a road tunnel are well documented in the literature. Human behaviour during a fire is loosely predictable; neither the egress time nor fire characteristics can be accurately predicted. Fires depend on fuel or ventilation to burn. The time to extinguish a fire event depends on the fire suppression techniques utilized, such as ventilation at negative pressure, water sprinklers, and embedded fire extinguishing devices. For case study purposes, the occurrence likelihood of a fire is not considered here; instead, fire risk is conditioned on certain design-based fire scenarios.

Fire intensity depends on the amount of available fuel. Hence, the fire size is directly proportional to the number and type of vehicles involved in the collision. While a typical car contributes a peak combustion energy of roughly 5 MW, an HGV (heavy goods vehicle) can contribute an average combustion energy of 50 MW, and, in certain cases, as much as 200 MW depending on the cargo

[21]. Therefore, Table 6 lists the five fire events and their associated risk scores considered in this thesis based on the study by Lonnermark and Ingason [33].

Table 6: Fire Scenarios Based on Vehicle Fuel

Collision Case	Estimated Fuel (MW)	Risk Score / 1
Single car Combustion	5	0.05
Car – Car Collision	10	0.10
Single HGV Combustion	50	0.50
Car – HGV Collision	55	0.55
HGV – HGV Collision	100	1.00

5.2 Case Study Analysis

Geospatial analysis of the above-mentioned variables is conducted using the developed ArcGIS map. Figure 14 shows the proposed locations of egress points and ramp exit points, the latter of which can also serve as additional egress points. Considering tunnel stations at a resolution of 100 m per station, the minimum distance from each station to the egress is provided in Table 7 for the first 10 stations. The distribution of the distance data for all stations can be further regressed using a lognormal function, as shown in Figure 15. From this distance distribution function, a relative risk model is developed for egress in Table 8 using the inverse normal relationship, such that the 100% exceedance probability corresponds to a risk score of 0, 50% corresponds to 5, and 10% corresponds to 9, among others.

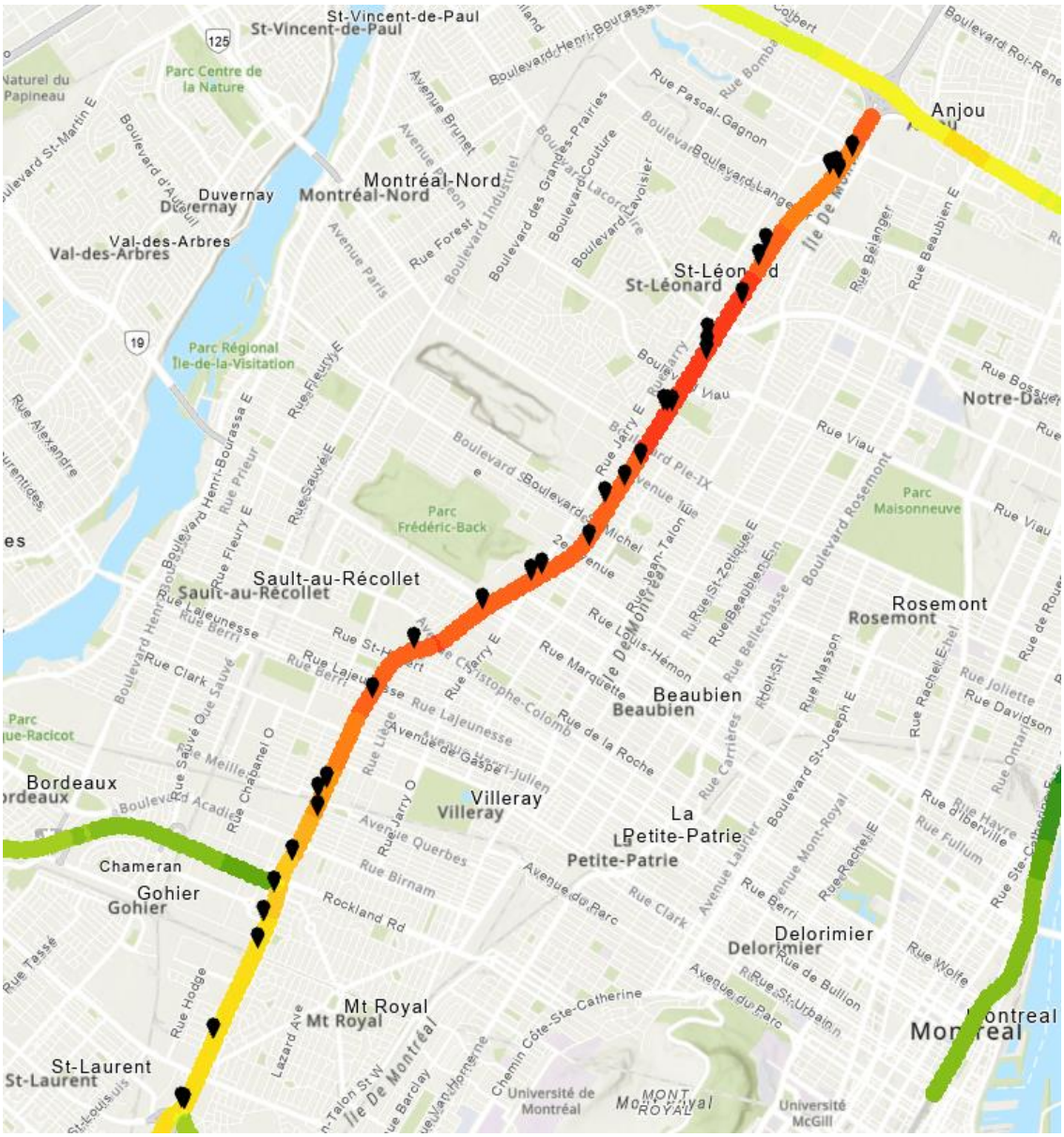

Figure 14: Egress Locations (black marker) for the Considered Tunnel

Table 7: Distances to Nearest Egress for Each Station

Station (Each 100 m)	X	Y	Nearest Egress	D to Nearest Egress (m)
1	299483	5051432	[ANJOU]	100.0
2	299430	5051349	[ANJOU]	200.0
3	299379	5051265	[LANGELIER E]	285.9
4	299326	5051177	[LANGELIER E]	185.9
5	299276	5051084	[LANGELIER E]	85.9
6	299222	5051004	[LANGELIER E]	56.8

7	299163	5050923	[EI1]	120.5
8	299113	5050837	[EI1]	20.5
9	299053	5050759	[EI1]	78.4
10	298988	5050679	[EI1]	178.4

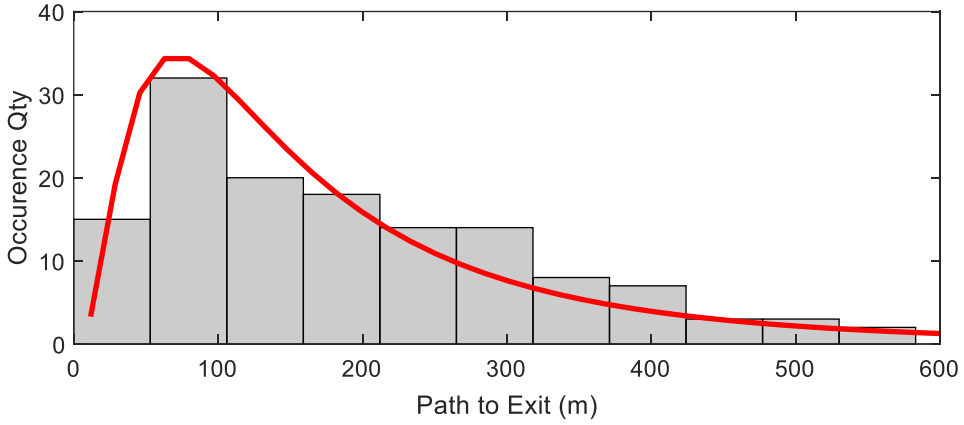

Figure 15: Lognormal Regression of Egress Data

Table 8: Risk Scoring Matrix for Egress

Egress Distance Statistics	**Mean (m)**	**St. Deviation (m)**
	198.88	198.05
Risk Score	**Distance Range (m)**	**Probability of Exceedance**
1	< 32.20	90%
2	32.20 – 95.02	80%
3	95.02 – 148.71	70%
4	148.71 – 198.88	60%
5	198.88 – 249.10	50%
6	249.10 – 302.74	40%
7	302.74 – 365.56	30%
8	365.56 – 452.69	20%
9	452.69 – 659.61	10%
10	> 659.61	1%

Likewise, the fire engine delivery time is also analyzed using the inventory map that considers the minimum roadway path between the nearest fire station and the fire accident occurring at each tunnel station, as shown in Figure 16 for one example station. This distance travelled to reach the accident site is proportional to the delivery time for firefighting and hence the associated relative

risk score for fire damage. In particular, the fire station is connected to the nearest tunnel surface exit, and the fire location is connected to the nearest roadway entrance, to create the most efficient travel path. Hence, the delivery distance of firefighting is measured for each of the tunnel stations, as summarized in Table 9 for the first 10 stations. The distribution of the firefighting distance data for all tunnel stations is then regressed as a normal distribution, as shown in Figure 17. This distribution was used as the basis for determining the risk scoring criteria for fire engine delivery time, as shown in

Table 10, using the inverse normal relationship that sets the boundaries for a scale out of 10.

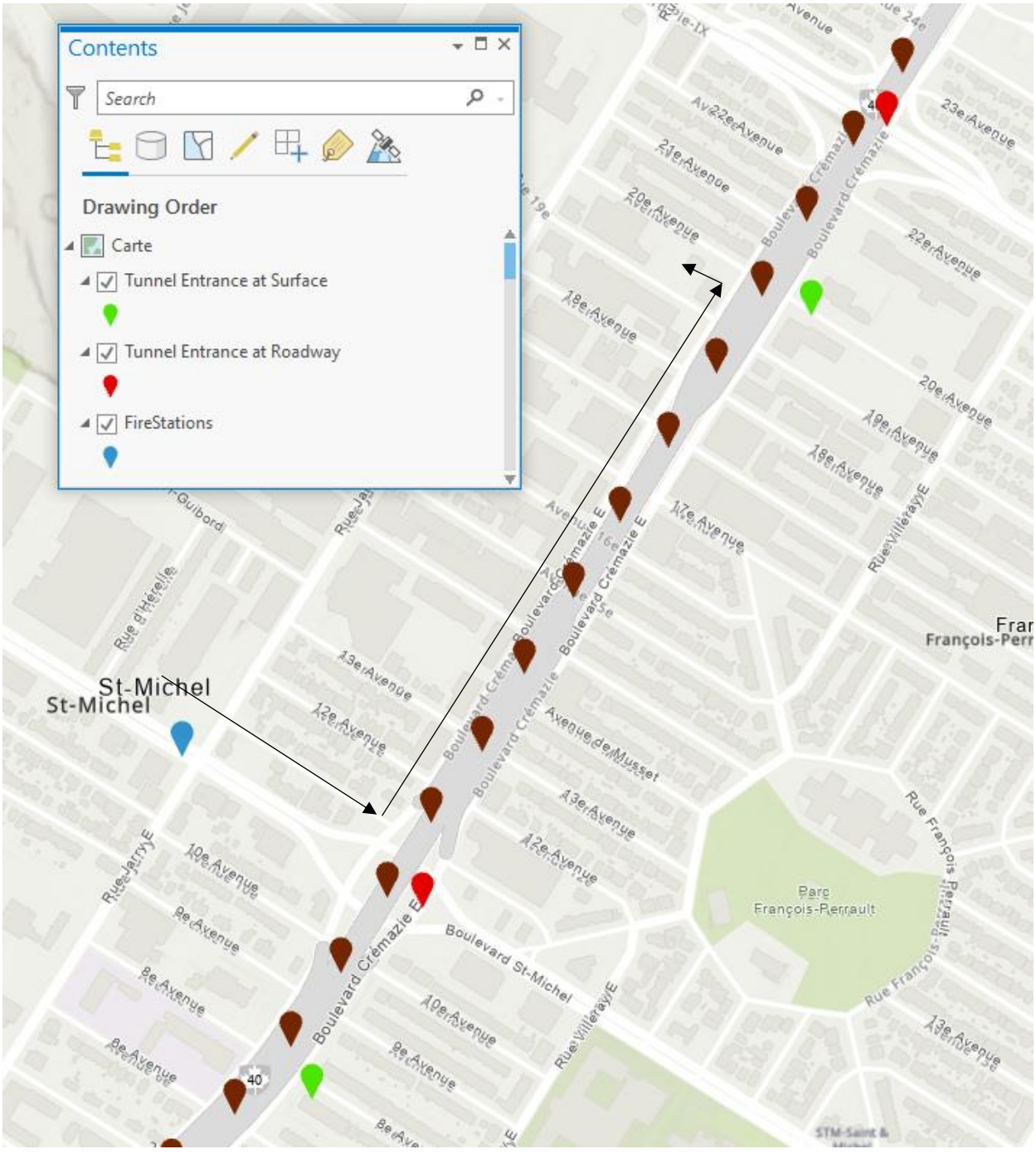

Figure 16: Minimum Fire Engine Path to Station 47, totalling 841.99m

Table 9: Distances to Fire Stations for the first 10 Tunnel Stations

STATION	X	Y	Nearest Fire Station	D to Nearest Fire Station (m)
1	299483	5051432	28	2057.97
2	299430	5051349	28	1957.97
3	299379	5051265	28	1857.97
4	299326	5051177	28	1757.97
5	299276	5051084	28	1657.97
6	299222	5051004	28	1557.97
7	299163	5050923	28	1657.97
8	299113	5050837	28	1757.97
9	299053	5050759	28	1857.97
10	298988	5050679	28	1957.97

Table 10: Fire Station Proximity Statistics

FIRE STATION DIST. STATISTICS	**Mean**	**St. Deviation**
	1954.38	742.06
Risk Score	**Value Range**	**Probability of Exceedance**
1	< 1003.39	90%
2	1003.39 – 1329.85	80%
3	1329.85 – 1565.24	70%
4	1565.24 – 1766.38	60%
5	1766.38 – 1954.38	50%
6	1954.38 – 2142.38	40%
7	2142.38 – 2343.52	30%
8	2343.52 – 2578.92	20%
9	2578.92 – 2905.37	10%
10	> 2905.37	1%

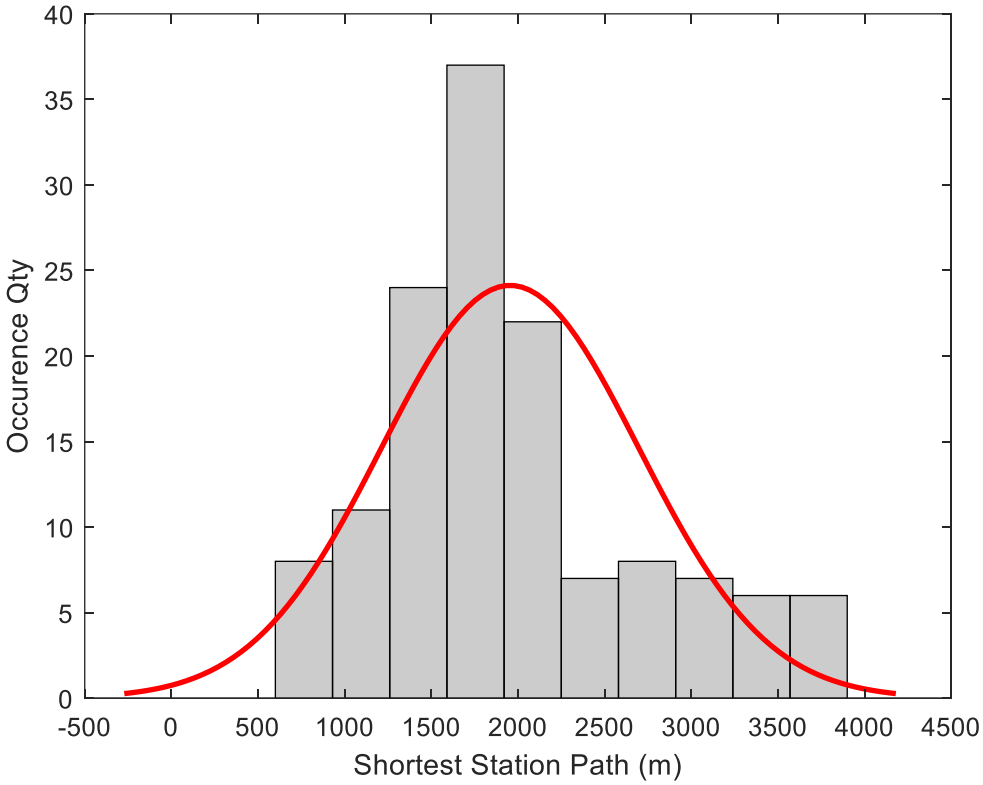

Figure 17: Histogram of Fire Station Proximity With Normal Regression

5.2 Fire Risk Assessment

The fire risk of the considered road tunnel is assessed by computing the combined effect from the fire event, traffic condition, accessibility to safe exit points, and right of way for fire engines. To this end, a combined risk index needs to be designed to assess the relative risk across all tunnel stations. First, as discussed in Section 5.1, the risk score for the design-level fire intensity is based on the fire fuel. The score ranges from 0.1 to 1.0 when the fuel is increased from 0 to 100 MW, as shown in Table 6. Second, risk scores for the distance to egress and delivery time of the fire engine are provided in Table 8 and Table 10 and are multiplied to produce a combined score for the "positional risk factor" from 1-100 for a given fire event. As such, the final risk score can now be tabulated for each tunnel station if the inputs of collision type, egress proximity, and fire engine

delivery distance are known. The “positional risk factor” is shown in Table 11 for the first 10 stations of the road tunnel. This risk factor can then be adjusted to different fire events by further multiplying it with the risk score for fire intensity.

Table 11: Nominal Risk Scores for the First 10 Tunnel Stations

STATION	X	Y	RISK SCORE
1	299483	5051432	18
2	299430	5051349	30
3	299379	5051265	30
4	299326	5051177	16
5	299276	5051084	8
6	299222	5051004	6
7	299163	5050923	12
8	299113	5050837	4
9	299053	5050759	10
10	298988	5050679	24

With a risk index prepared, the inventory analysis of the proposed tunnel can be updated to communicate, using a relative scoring scheme, the peak design risk from fire at each station along the tunnel’s length. First, the relative occurrence of different fire scenarios must be considered for the five cases mentioned in Table 6. Based on the relative frequency of different vehicle types along the roadway of 25% trucks and 75% cars, it can be assumed with equal accident risk that accident likelihood is proportional to vehicle presence, and that single vehicle fires and like-vehicle collisions are equally likely. Such, a single factored score accounting for the relative frequency of vehicles proportional to their fire outcome can be computed for 3 scenarios:

(1) Unadjusted Risk Score Modifier (no vehicle-type discounting);

$$Vehicle\_Modifier_1 = 1$$

(2) Vehicle-Adjusted Risk Score (expected risk)

$$Vehicle\_Modifier_2$$

$$= \left[\sum (vehicle\ 1\ occurence\ \%) * (vehicle\ 2\ occurence\ \%) * (risk\ multiplier)\right]/3$$

$$= (0.25 * 0.25 * 1.0 + 0.25 * 0.5 + 0.25 * 0.75 * 0.55)/3 + (0.75 * 0.75 * 0.1 + 0.75$$

$$* 0.25 * 0.55 + 0.75 * 0.05)/3 = 0.1625$$

(3) Car-Only Adjusted Risk Score, with the assumption that trucks will be banned from the tunnel and be rerouted to a surface boulevard (expected risk without trucks).

$$Vehicle_{Modifier_3}$$

$$= Avg.of\ car\ fire\ risk\ multipliers$$

$$= 0.5 * M1 + 0.5 * M2$$

$$0.5 * 0.05 + 0.5 * 0.1 = 0.075$$

In consideration of these discounting scores, the factored risk score can be produced for each station of the proposed system. In Table 12 below, the final risk scores for the first 10 stations are tabulated for the nominal and the two discounted risk rates.

Table 12: Risk Scores Summary for the First 10 Tunnel Stations

STATION	X	Y	NOMINAL RISK SCORE	ALL VEHICLE NET SCORE	NO TRUCK NET SCORE
1	299483	5051432	18	2.925	1.35
2	299430	5051349	30	4.875	2.25
3	299379	5051265	30	4.875	2.25
4	299326	5051177	16	2.6	1.2
5	299276	5051084	8	1.3	0.6
6	299222	5051004	6	0.975	0.45
7	299163	5050923	12	1.95	0.9
8	299113	5050837	4	0.65	0.3
9	299053	5050759	10	1.625	0.75
10	298988	5050679	24	3.9	1.8

Subsequently, the full results of the risk indexing for each of the three vehicle modifier cases and component scores are given in Appendix II: Full Nominal Risk Results. Shown below in Figure 18 is the raster of the overall nominal risk score across the proposed corridor.

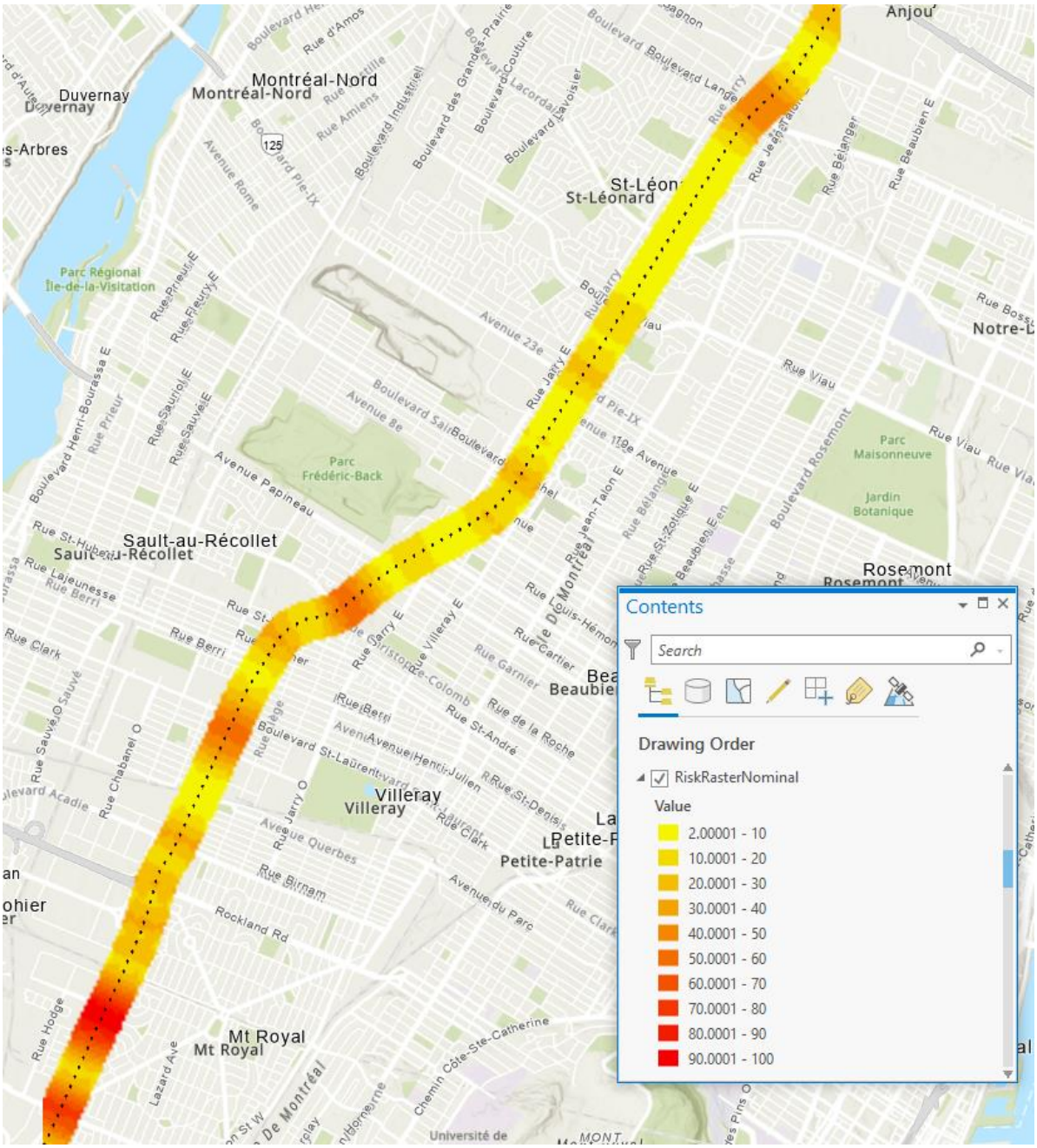

Figure 18: Raster of Nominal Risk Scores with Legend

Because the vehicle types are not geospatial, they can be omitted from this map; nonetheless, the analysis of vehicle types concludes that the risk factor due to vehicle type drops by 53.1% if trucks are rerouted from the tunnel.

5.3 Fire Risk Results and Discussions

Composing a case study to investigate fire risk across a proposed road tunnel yields some key observations. First, the overall fire risk of the tunnel will be reduced by 54% if the truck traffic is rerouted to a surface boulevard. This is achieved by reducing the size of possible fire events. This solution also alleviates potential traffic congestion in the tunnel and has been established for road tunnels with heavy traffic, such as the George Wallace Tunnel in Mobile, AL [34]. Second, the case study produced a full geospatial fire risk map for all stations along the proposed tunnel corridor. Using the established inventory analysis strategy, a raster can also be employed to interpolate the risk results at intermediate locations, as presented in Figure 18. Furthermore, the risk map allows the end user to make interactive, dynamic risk mitigation decisions, as discussed below.

Using the ArcGIS-based fire risk map, users can explore the effectiveness of different risk mitigation strategies. For example, one can add a new fire station near the station that has the highest risk, namely at coordinates (291987, 5040288), the intersection of Chemin Duncan and Decarie Boulevard. The risk results can then be re-calculated, as shown in Figure 19, where the peak fire risk is reduced from 100 at station 122 to 60 at station 93. This is one of many potential design decisions that can be made to reduce the fire risk of the tunnel.

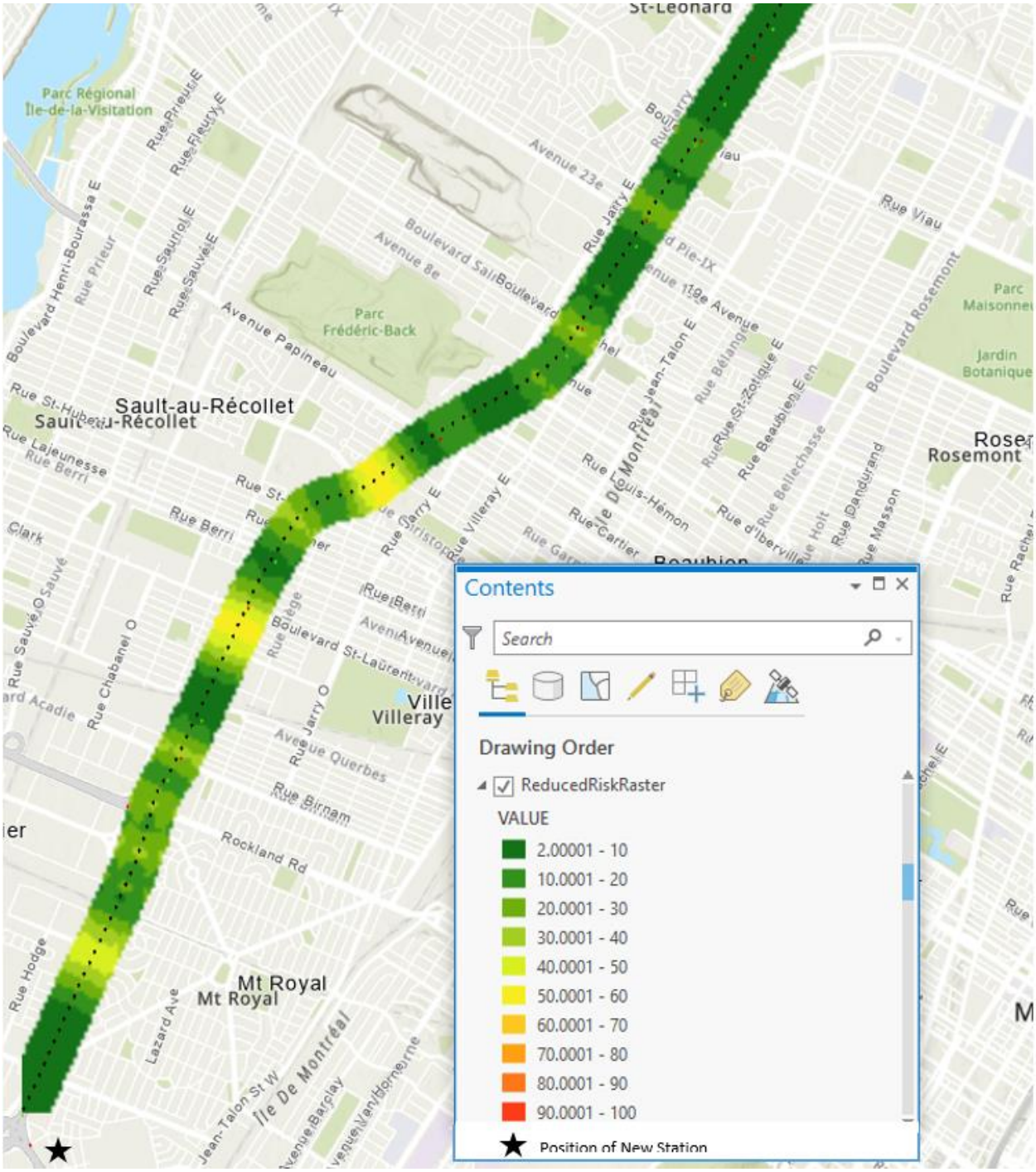

Figure 19: Reduced Risk Map with Additional Fire Station denoted by Star, bottom left

Chapter VI: Conclusions and Future Work

A thorough soil database and inventory management system has been developed in ArcGIS with supporting data presented in excel spreadsheets. Using established information on the soil characteristics and geographical constraints of Montreal, a foundational system to risk-assess any hazard was produced.A case study was performed to evaluate the relative risk from fire at each station along a proposed road tunnel corridor with several design assumptions. Using this case study, the locations on the proposed right-of-way most in danger of fires and the ideal location for a new fire station were determined. It was also found that all causes of fire could be reduced by 54% simply by re-routing heavy truck traffic outside this tunnel. In this section, the validity of the assumptions and the potential improvements to this process for subsequent work are discussed, and the results of the study are reviewed.

The inventory analysis system developed in this thesis was used primarily to make geospatial measurements and to generate statistical analyses on which to validate the work and to ultimately make engineering judgement decisions. Despite limited inputs and a low resolution of 100m station frequencies, the case study demonstrating this system was still able to produce a relative risk score based on validated empirical criteria at the same resolution as the inputs given from prior studies in order to find the highest-risk positions along the tunnel. Furthermore, the results of this approach were used to place a new fire station, reducing the peak risk score from 100 to 60 for the network. Although this is a rough design scheme, this 40% reduction in risk was a mitigation decision made possible by the data processing and interactive mapping of the ArcGIS inventory analysis system.

For future work, there are many opportunities to use the other parameters included in the design of the inventory analysis to expand a case study beyond the limited scope of fire safety to include

all design risk scenarios. Following code requirements, this system could also be used to combine the factored load effects of various risks simultaneously to evaluate a theoretical ultimate limit state and understand how risk interventions affect the overall design safety in real conditions. Moreover, this work is intended as the starting point for a further study into the seismic risks of the overall network of tunnels in the Montreal region and design interventions to minimize these risks in an efficient manner. To understand and interact with risk analysis in a geospatial database tool ultimately allows the user no limit to useful applications that can extend from this preliminary work.

The accuracy of the inventory analysis system designed and subsequently used to discuss risk mitigation in this thesis is subject and sensitive to the accuracy of the input conditions specified. Station frequencies of 100m, rudimentary design values for traffic frequency, and rough assumptions for the delivery time of emergency vehicles all limit the validity of the numbers produced in the case study. However, the intention of the case study to demonstrate the ability to understand and process data inputs to make informed risk decisions was a success, and this system could ultimately be extended, with the improved accuracy of input data produced by real-life investigative studies and survey work, as a strategy to be used in construction to minimize the cost and scope of design interventions while still targeting the highest risk positions in a network of tunnels or similar infrastructure.

References

[1] Centre for New Urbanism, "The Life and Death of Urban Highways," Centre for New Urbanism, 2012.

[2] Montreal Gazette, "Transport Quebec Plans to Rebuild 5km of the Metropolitain," Montreal Gazette, 12 January 2020. [Online]. Available: https://montrealgazette.com/news/local-news/transport-quebec-plans-to-rebuild-5-km-of-the-metropolitan. [Accessed 3 March 2023].

[3] L. Gyulai, "Tunnel the Met: An idea that keeps resurfacing," Montreal Gazette, Montreal, 2022.

[4] National Academy of Engineering, Completing the "Big Dig": Managin the Final Stages of Boston's Central Artery/Tunnel Project, Washington, DC: The National Academic Press, 2003.

[5] D. B. L. Jr., "Induced Traffic and Induced Demand," N.D.. [Online]. Available: https://nacto.org/docs/usdg/induced_traffic_and_induced_demand_lee.pdf. [Accessed 30 March 2023].

[6] D. B. Lee Jr., "Induced Traffic and Induced Demand," National Association of City Transport Officials.

[7] G. Duranton and M. A. Turner, "The Fundamental Law of Road Congestion: Evidence from U.S. Cities," *American Economic Review*, vol. 101, pp. 2616 - 2652, 2011.

[8] D. A. Hensher, Urban Transport Economics, Cambridge: Cambridge University Press, 1977.

[9] Mass.Gov, "The Big Dig: Project Background," Government of Massachussets, 2023. [Online]. Available: https://www.mass.gov/info-details/the-big-dig-project-background. [Accessed 9 March 2023].

[10] Boston Magazine, "Then and Now: Menino's Boston," Boston Magazine, 24 September 2013. [Online]. Available: https://www.bostonmagazine.com/news/2013/09/24/mayor-tom-menino-big-dig-photos/. [Accessed 26 February 2023].

[11] R. Slade, "Then and Now: Menino's Boston," City Life, 24 September 2013. [Online]. Available: https://www.bostonmagazine.com/news/2013/09/24/mayor-tom-menino-big-dig-photos/. [Accessed 5 March 2023].

[12] R. Khalil, "Decision support system for tunnel alignment based on GIS," *Civil Engineering Research Magazine,* pp. 656-667, 2013.

[13] S. A. R. Shah, T. Brijs, N. Ahmad, A. Pirdavani, Y. Shen and M. A. Basheer, "Road Safety Risk Evaluation Using GIS-Based Data Envelopment Analysis," *Applied Sciences*, 2017.

[14] L. Griffin, "Analyzing car crashes in space and time," ArcGIS, 2021.

[15] S. Wang, L. Mu, M. Qi, Z. Yu, Z. Yao and E. Zhao, "Quantitative risk assessment of storm surge using GIS techniques and open data," *Journal of Environmental Management,* vol. 289, 2021.

[16] M. Schubert, N. P. Hoj, A. Ragnoy and H. Buvik, "Risk Assessment of Road Tunnels using Bayesian Networks," *Procedia - Social and Behavioral Sciences,* vol. 48, pp. 2697-2706, 2012.

[17] M. Holicky, "Reliability analysis for structural design," Sun Press, Stellenbosch, 2009.

[18] T. P. Thaker, P. K. Savaliya, M. K. Patel and K. A. Patel, "GIS Based Seismic Risk Analysis of Ahmedabad City, India," in *Proceedings of GeoShanghai 2018 International Conference: Geoenvironment and Geohazard*, Shanghai, 2018.

[19] D. Toma-Danila, L. Armas and A. Tiganescu, "Network-risk: an open GIS toolbox for estimating the implactions of transportation network damage due to natural hazards, tested for Bucharest, Romania," *Natural Hazards and Earth System Sciences*, pp. 1421-1439, 2020.

[20] F. Tarada and M. King, "Structural Fire Protection of Railway Tunnels," in *Railway Engineering Conference, University of Westminister UK*, Westminister, 2009.

[21] J. Gehandler, "Road tunnel fire safety and risk: a review," *Fire Science Reviews*, vol. 4, no. 2, 2015.

[22] GeoScape Montreal, "A Billion Years of History Montreal," Geological Survey of Canada, Montreal, 2002.

[23] V. Prest, "Geology and Engineering Characteristics of Surficial Deposits, Montreal Island and Vicinity," Montreal, 1977.

[24] Society de Transport a Montreal, "Forages BTM," Montreal, 1966.

[25] L. Boyer, A. Bensoussan, M. Durand, H. Grice and J. Berard, "Geology of Montreal, Province of Quebec, Canada," Association of Engineering Geologists, 1985.

[26] L. Chouinard, P. Rosset, A. De La Puente, R. Madriz, D. Mitchell and J. Adams, "Seismic Hazard Analysis for Montreal," in *13th World Conference on Earthquake Engineering*, Vancouver, 2004.

[27] CBC, "At 50, the Louis-Hippolyte-La Fontaine bridge-tunnel still a world-class wonder," 11 March 2017. [Online]. Available: https://www.cbc.ca/news/canada/montreal/at-50-the-louis-hippolyte-la-fontaine-bridge-tunnel-still-a-world-class-wonder-1.4021079. [Accessed 6 March 2023].

[28] TomTom, "Montreal Traffic Study," TomTom, 14 January 2023. [Online]. Available: tomtom.com/traffic-index/montreal-traffic . [Accessed 14 January 2023].

[29] ESRI Documentation, "Pop-ops, ArcGIS Pro 3.0," ESRI, 2023. [Online]. Available: https://pro.arcgis.com/en/pro-app/3.0/help/mapping/navigation/pop-ups.htm#:~:text=The%20Pop%2Dup%20pane%20displays,of%20attributes%20all%20the%20time.. [Accessed 12 March 2023].

[30] Z. Li, M. Smirnova, Y. Zhang, N. Smirnov and Z. Zhu, "Tunnel speed limit effects on traffic flow explored with a three lane model," *Mathematics and Computers in Simulation,* vol. 194, pp. 185-197, 25 November 2021.

[31] L. Moore-Merrell, "Understanding and Measuring Fire Department Response Times," Lexicon, 17 July 2019. [Online]. Available: https://www.lexipol.com/resources/blog/understanding-and-measuring-fire-department-response-times/. [Accessed 24 May 2023].

[32] US DOT, "Technical Manual for Design and Construction of Road Tunnels," US DOT, New York City, 2009.

[33] A. Lonnermark and H. Ingason, "Fire Spread and Flame Length in Large-Scale Tunnel Fires," *Fire Technology,* vol. 42, pp. 283-302, 2006.

[34] AP News, "Truckers Fume as Alabama Detours them from I-10 Tunnel," AP News, 2021.

[35] Stantec, "Etude Geotechnique et caracterisation environmental," Stantec, Saint Laurent, 2017.

[36] A. Rancourt, "Design and Construction of sharts and hard rock TBM Tunnel for a water main in Montreal," in *TAC2014*, 2019.

[37] Z. Brisevac, D. Pollak, A. Maricic and A. Vlahek, "Modulus of elasticity for grain-supported carbonates - determination and estimation for preliminary engineering," vol. 11, no. 13, 2021.

[38] M. Bai, "Why are brittleness and fracability not equivalent in designing hydraulic fracturing in tight shale gas reservoirs," *Petroleum,* vol. 2, no. 1, pp. 1-19, 2016.

[39] Q. Li, M. Chen, Y. Jin, Y. Zhou, F. Wang and R. Zhang, "Rock mechanical properties of shale gas reservoir and their influences on hydraulic fracture," in *Society of Petroleum engineers - international petroleum technology Conference*, 2013.

[40] B. Vasarhelyi, "A possible method for estimating the Poisson's ratio values of the rock masses," *Acta Geodetica et Geophysica Hungarica,* vol. 44, no. 3, pp. 313-322, 2009.

[41] A. Selvadurai, "Geomechanical Characterization of the CObourg Limestone," NWMO, Montreal, 2017.

[42] Nuclear Waste Management Organization, "Regional Geomechanics - Southern Ontario," NWMO, 2011.

[43] M. Arif, "Displacement Analysis of Sheet Pile with Tie Beam on Breakwater Construction using PLAXIS," 2020.

[44] A. Beaudoin, "Adapted Soil Properties Reference Values," Montreal, 2022.

[45] S. K. Thota, T. D. Cao and F. Vahedifard, "Poisson's Ratio Characteristic Curve of Unsaturated Soils," ASCE, 2020.

[46] H. Sahrma, M. Dukes and D. Olsen, "Field Measurements of Dynamic Moduli and Poisson's Ratios of Refuse and Underlying Soils at a Landfill Site," *Geotechnics of Waste Fills - Theory and Practice*, pp. 57-70, 1990.

[47] Obrzud, Truty and Kezdi, "Soil Young's Modulus," Geotech Data, 2013.

[48] D. Wyllie and N. Norrish, Rock Strength Properties and Their Measurement: Investigation and Mitigation, 2017, p. 372.

[49] M. Talukder, "Seismic Site Effects for the Island of Montreal," McGill University, Montreal, 2018.

[50] J. Sun, R. Golesorkhi and H. Seed, "Dynamic Moduli and Damping Ratios for Cohesive Soils," Earthquake Engineering Research Centre, Berkeley, 1988.

[51] H. Seed, "Soil Moduli and Damping Factors for Dynamic Response Analysis," *EERC*, 1970.

[52] H. Seed, "Moduli and Damping Factors for Dynamic Analyses of Cohesionless Soils," *Journal of Geotechnical Engineering,* vol. 112, no. 11, pp. 1016-1032, 1986.

[53] P. Rosset, M. Bour-Belvaux and L. Chouinard, "Microzonation Models for Quebec with Respect to Vs30," *Bulletin of Earthquake Engineering,* vol. 13, no. 8, pp. 2225-2239, 2015.

[54] K. Rasmussen, "An investigation of monotonic and cyclic behaviour of Leda Clay".

[55] H. Javdanian, "Assessment of shear stiffness ration of cohesionless soils using neural modeling," *Modelling Earth Systems and Envrionment,* vol. 3, pp. 1045-1053, 2017.

[56] M. Durand, "Classifications des phenomenes et cartographie geotechnique des roches recontrees dans les grand travaux urbains a Montreal, Canada," in *III International Congress, Section 1, Regional Planning,* Madrid, Spain, 1978.

[57] P. Daneshvar and N. Bouaanani, "Damping modification factors for eastern Canada," *Journal of Seismology,* vol. 21, pp. 1487-1504, 2017.

[58] M. Carter and S. Bentley, Correlations of Soil Properties, Pentech Press Publishers, 1991.

[59] R. Bauer, "Shear Wave Velocity, Geology and Geotechnical Data of Earth Minerals in the Central US Urban Hazard Mapping Areas," USGC External Grant, 2007.

[60] K. K. Banab, "Seismic site response analysis for Ottawa, Canada: a comprehensive study using measurements and numerical simulations," *Bulletin of the Seismological Society of America,* vol. 102, no. 5, pp. 1976-1993, 2012.

[61] National Research Council of Canada, "National Building Code of Canada," Canadian Commission on Building and Fire Codes, Ottawa, 2020.

[62] ABS, "Etude Geotechnique, Hydrogeologique et Caracterisation Environmentale des Sols," ABS, Montreal, 2019.

[63] J. P. Bocarejo, M. C. LeCompte and J. Zhou, "The Life and Death of Urban Highways," ITDP, 2012.

[64] A. Rancourt, "Design and Construction of shafts and hard rock TBM Tunnel for a water main in Montreal," in *TAC2014*, 2019.

[65] A. Selvadurai, "Geomechanical Characterization of the Cobourg Limestone," NWMO, Montreal, 2017.

[66] F. Dall'Osso, A. Cavalletti and P. Polo, "Risk Assessment and Evaluation ArcGIS Toolbox," Italian Ministry for the Environment and Territory, Rome.

Appendix I: Soil Database Reference Information

Rock and Soil Properties

Different data resources are considered to synthesize a database for determining the rock and soil properties. As shown in Table 13, a data rating system is developed to quantify the data quality associated with each property parameter. The rating category, ranging from A – D, is determined based on the closeness of the data resource to the geological condition of the Island of Montreal. Accordingly, Table 14 summarizes the statistics of the soil and rock properties that will be used as data inputs for finite element modelling and regional risk assessment. Detailed discussions for determining the properties of the rock and each soil type are provided below.

Table 13. Rating System for Constituent Soil Properties

Rating	**Note**
A	Data interpreted and extracted directly from sourced borehole studies
B	Data from the literature specific to the island of Montreal
C	General properties of soils/rocks with an indirect relation to the island of Montreal
D	General soil properties with no proven relation to Montreal geology

Table 14. Statistics of soil/rock properties

Soil Type	Parameter	Distribution				Data Quality
		Type	μ	σ	Range	
Rock	E (GPa)[1]	Normal	56.2	12.2	31.8 – 80.7	A
	ν[2]	Normal	0.29	0.01	0.27 – 0.31	A
	C (MPa)[3]	Normal	28.0	4.5	19.0 – 37.0	C
	φ[4]	Normal	38.0	2.0	34.0 – 42.0	C
	γ (kN/m^3)[5]	Normal	26.5	0.7	25.1 – 28.0	A
Gravel	E (GPa)	Normal	120	20	80.0 – 160.0	C
	ν	Normal	0.4	0.04[6]	0.33 – 0.49	B
	C (kPa)	-	-	-	-	A

	φ	Normal	33.0	3.3[6]	26.4 – 39.6	A
	γ (kg/m^3)	Lognormal	7.8	0.08	7.6 – 7.9	A
Sand	*E* (GPa)	Normal	40	5	30.0 – 50.0	C
	ν	Normal	0.25	0.05	0.15 – 0.35	B
	C (MPa)	-	-	-	-	A
	φ	Normal	36.0	3.6[6]	28.8 – 43.2	A
	γ (kN/m^3)	Lognormal	7.7	0.05	7.6 – 7.8	A
Silt	*E* (GPa)	Normal	16	2	12.0 – 20.0	C
	ν	Normal	0.2	0.02[6]	0.15 – 0.23	B
	C (MPa)	-	-	-	-	A
	φ	Normal	30.0	3.0[6]	24.0 – 36.0	A
	γ (kN/m^3)	Lognormal	7.7	0.08	7.5 – 7.9	A
Clay	*E* (GPa)	Normal	6.5	0.75	5.0 – 8.0	C
	ν	Normal	0.33	0.06	0.20 – 0.45	B
	C (MPa)	Normal	57.5	16.8	24.0 – 91.0	A
	φ	Normal	26	2.6[6]	20.8 – 31.2	D
	γ (kN/m^3)	Lognormal	7.6	0.14	7.4 – 7.9	A

[1] Young's Modulus; [2] Poisson's ratio; [3] Cohesion; [4] Friction angle; [5]Unit Weight; [6]10% coefficient of variation is assumed due to the lack of data

Rock

Three references are collected to determine the Young's Modulus, Poisson ratio, and unit weight of the rock material. These include soil borehole data provided by STM [24] [35] and a previous study conducted by Boivin et al. [36]. Data points from the soil borehole data are digitized, summarized, and regressed against normal or lognormal distribution functions, and the statistical parameters of these regressed distributions are validated with relevant information reported by Boivin et al. [36].

Correlations have also been considered among different rock properties. For instance, Brisevac et al. [37] showed that the rock density is related to Young's modulus in collected rocks. The negative linear relationship between Young's modulus and Poisson ratio has been investigated by Bai [38]

and Li et al. [39]. These studies indicated that the correlation coefficient between Young's modulus and density is around 0.54, whereas a negative correlation of -0.50 has been reported between Young's modulus and Poisson ratio. Furthermore, Vásárhelyi [40] proposed that the rock's internal friction angle and Poisson ratio follow a linear curve relationship.

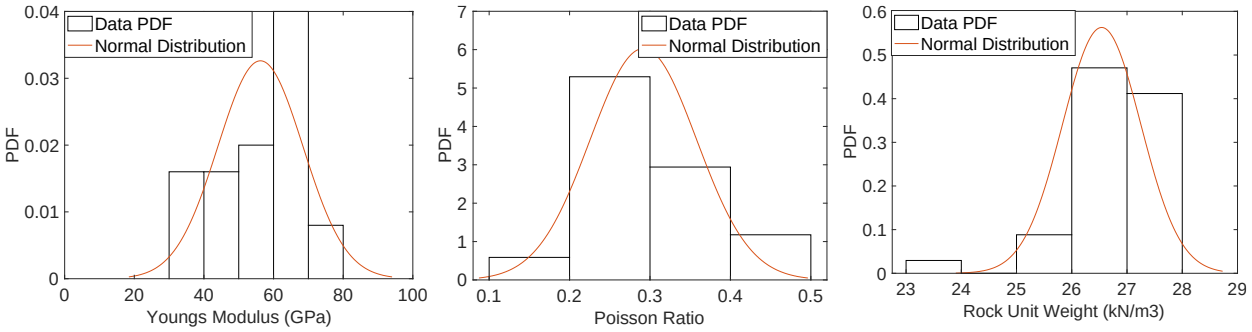

(a) (b) (c)

Figure 20. Normal Trends for Rock Data

Figure 20 (a) shows the statistical fit of the Young's Modulus toward a normal distribution with a mean value of 56.2 GPa and a standard deviation of 12.2 GPa. The data range is consistent with those reported by Boivin et al. [36] for limestone (i.e., mean value at 55 GPa with a range of 7-92 GPa), as shown in Table 9. Likewise, data for the Poisson ratio is regressed to have a normal distribution with a mean value of 0.29 and a standard deviation of 0.06 in Figure 20 (b), which agrees with the range (0.04-0.41 with a mean of 0.23) reported by Boivin et al. [36] (Table 15). Note that enforcing the correlations among rock properties leads to a smaller range of values for the Poisson ratio, as listed in Table 14. A normal distribution can also be used to fit the bulk unit weight data of rock, resulting in a mean of 26.5 kN/m^3 and a standard deviation of 0.7 kN/m^3 in Figure 20 (c). Similarly, Table 15 lists that the volumetric mass for rock has a mean of 26.5 kN/m^3 and a range of 22.7-27.1 kN/m^3.

Table 15. Rock Properties from Boivin [36]

Property	**Unit**	**Rock type (average (min-max))**	
		Limestone	Intrusive
Volumetric mass	kN/m	26.5 (22.7-27.1)	27.5 (24.4-30.8)
Deformation module	GPa	55 (7-92)	72 (26-113)
Poisson ratio	-	0.23 (0.04-0.41)	0.28 (0.14-0.49)
USC	MPa	143 (44-306)	228 (108-431)

No relevant data has been found regarding the friction angle and cohesion for the limestone bedrock underlaying the island of Montreal. Alternatively, this study considers that the Cobourg limestone in the proximate Southern Ontario Canadian Shield shares similar properties. Triaxial tests have been performed by Selvadurai [41] to determine the failure stresses (σ_1) under different stress states (σ_3) for the Cobourg limestone. By defining a Mohr-Coulomb failure criterion of the limestone, a relationship between rock cohesion and friction angle can be established as:

$$\frac{\sigma_1 - \sigma_3}{2} = c\cos\varphi + \frac{\sigma_1 + \sigma_3}{2}\sin\varphi \quad (1)$$

One direct shear test has been conducted, indicating that the friction angle of the Cobourg limestone is 37° [42]**.** The friction angle range is different for various rock friction classes, which are related to the size and shape of the grains exposed on the fracture surface. It is reported that the typical friction angle range for limestone is from 34-42 degrees [43]. Selvadurai [41] conducted eight sets of failure tests for the Cobourg limestone to determine the Mohr-Coulomb failure criterion. The measured stress states and the corresponding failure stress from Selvadurai [41] are utilized to predict the rock cohesion under each friction angle, depicted in Figure 21. The final

value for the rock cohesion is randomly selected from these eight sets of data under the given friction angle.

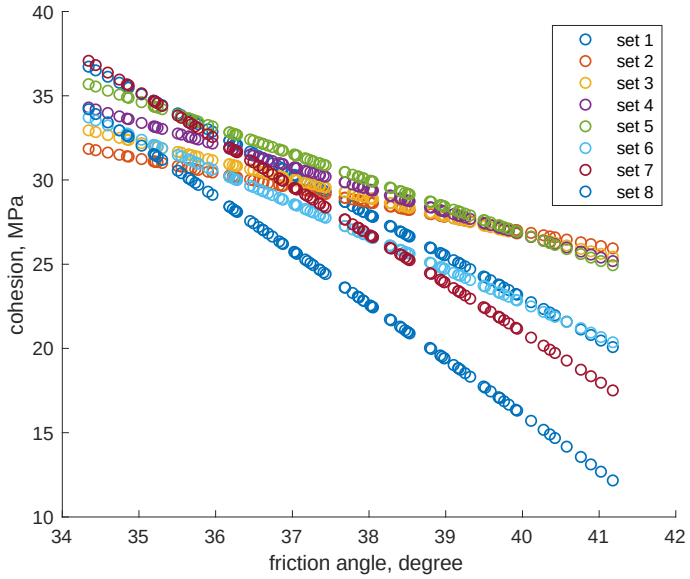

Figure 21. Predicted cohesions based on different stress states

Soil

The cohesive soils including clay and silt have been investigated by Beaudoin for the Montreal region [44]. As shown in Table 16, the value range of the undrained shear strength is assumed to have a normal distribution with the bounds constrained by plus/minus two standard deviations. As such, the normal distribution parameters for the cohesion of the clay can be determined.

Table 16. Cohesive Soil Properties for Montreal Region [44]

Property	Typical Value Range
Water Content (W)	21,9 to 68,0 %
Undrained Shear Strength (S_u)	24 to 91 kPa
Unrestrained Shear Strength Revamped (S_{ur})	3 to 12 kPa
Liquidity Limit (W_L)	26 to 77 %
Plastic Limit (W_P)	16 to 33 %
Plasticity Index (I_P)	9 to 53%

Personal communication with Beaudoin [44] also provides data information regarding the unit weight, friction angle, and cohesion for the granular soils of the Montreal region. As listed in Table 17, the unit weight data is compared and validated with those obtained from the soil borehole study, whereas the listed friction angles are considered mean values for each soil type. The study considers the cohesions of gravel, silt, and sand to be 0 kPa, which are subjected to further refinement should more relevant data sources are pinpointed.

Table 17. Granular Soil Properties for Montreal Region [44]

Parameters	Gravel	Silt	Sand
Bulk Unit Weight (kN/m^3)	19.2	18.5	21.5
Friction Angle (deg)	33	30	36
Cohesion (kPa)	0	0	0

Without finding relevant references that are specific to the soils at Montreal, previous studies conducted by Thota et al. [45] and Sahrma et al. [46] are surveyed to determine the normal distribution parameters for the Poisson ratios of four soil types. The corresponding value ranges are listed in Table 18.

Table 18. Poisson Ratio for Granular Soils

Soil Layer	Value Range [45]	Value Range [46]
Gravel	0.41	0.3-0.4
Sand	0.15-0.35	0.3-0.4
Silt	0.19	0.3-0.35
Clay	0.20-0.45	0.4-0.5

The Hardening Soil Guidebook from Obzurb & Truty (2012) and the Handbook of Soil Mechanics by Kezdi (1974) are considered general references to determine the Young's Modulus values for the four soil types, as listed in Table 19 [47].

Table 19. Young's Moduli for Reference Soil Layers [47]

Soil Layer	Young's Modulus ranges (MPa)
Gravel	80-160
Sand	30-50
Silt	12-20
Clay	5-8

The unit weight of each soil type is obtained from laboratory test data [24]. As shown in Figure 22, the density data information is digitized as histogram figures and further regressed as lognormal distributions.

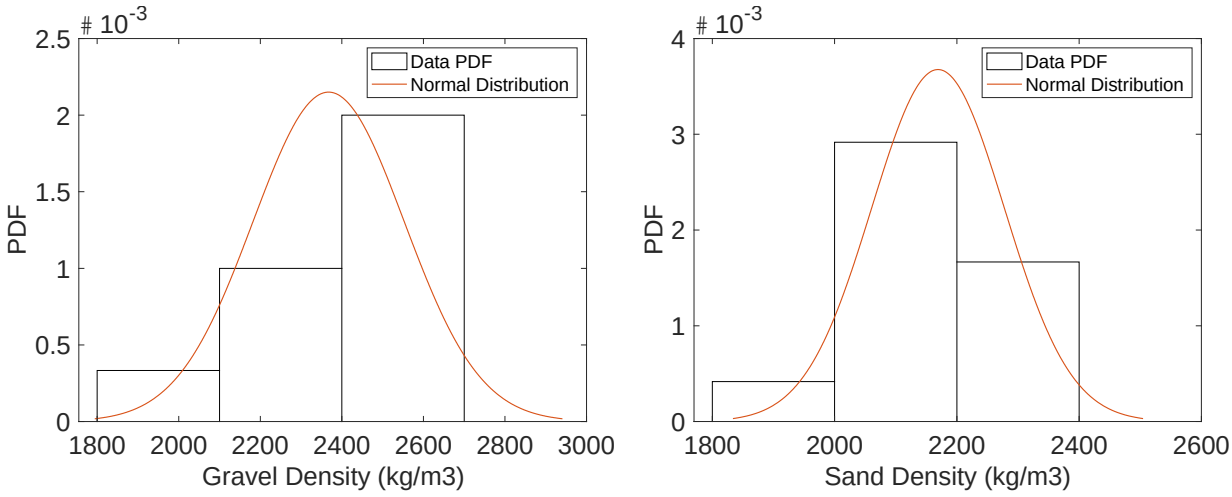

(a)

(b)

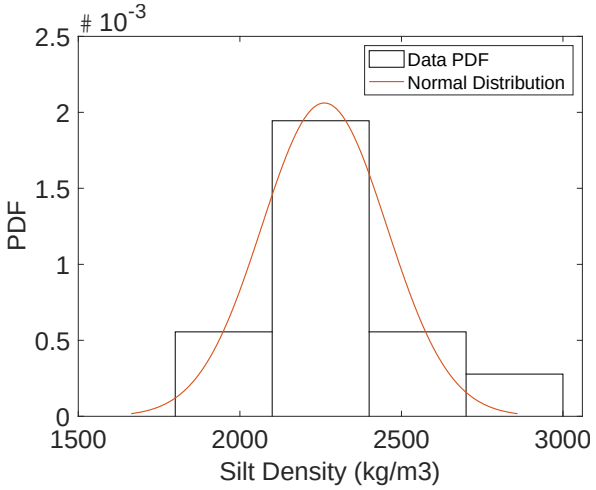

(c)

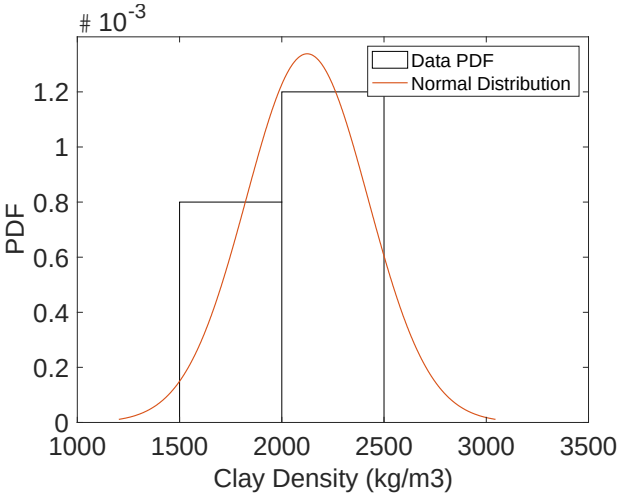

(d)

Figure 22. Statistical fits of the density of four soil types

Appendix II: Full Nominal Risk Results

Table 20: Full Risk Results Tabulated

STATION	X	Y	NOMINAL RISK SCORE	ALL VEHICLE NET SCORE	NO TRUCK NET SCORE	FIRE RISK SCORE	EGRESS RISK SCORE	D to Nearest Fire Station (m)	D to Nearest Egress (m)
1	299483	5051432	18	2.925	1.35	6	3	2057.97	100
2	299430	5051349	30	4.875	2.25	6	5	1957.97	200
3	299379	5051265	30	4.875	2.25	5	6	1857.97	285.92
4	299326	5051177	16	2.6	1.2	4	4	1757.97	185.92
5	299276	5051084	8	1.3	0.6	4	2	1657.97	85.92
6	299222	5051004	6	0.975	0.45	3	2	1557.97	56.78
7	299163	5050923	12	1.95	0.9	4	3	1657.97	120.5
8	299113	5050837	4	0.65	0.3	4	1	1757.97	20.5
9	299053	5050759	10	1.625	0.75	5	2	1857.97	78.37
10	298988	5050679	24	3.9	1.8	6	4	1957.97	178.37
11	298917	5050610	36	5.85	2.7	6	6	2057.97	278.37
12	298848	5050536	48	7.8	3.6	6	8	2052.23	378.37
13	298771	5050472	50	8.125	3.75	5	10	1952.23	478.37
14	298698	5050403	50	8.125	3.75	5	10	1852.23	573.98
15	298626	5050332	40	6.5	3	4	10	1752.23	473.98
16	298561	5050257	32	5.2	2.4	4	8	1652.23	373.98
17	298503	5050175	18	2.925	1.35	3	6	1552.23	273.98
18	298451	5050094	12	1.95	0.9	3	4	1452.23	173.98
19	298393	5050008	6	0.975	0.45	3	2	1352.23	73.98
20	298339	5049923	4	0.65	0.3	2	2	1252.23	58.02
21	298288	5049839	4	0.65	0.3	2	2	1152.23	57.37
22	298237	5049753	4	0.65	0.3	2	2	1052.23	51.88
23	298180	5049670	4	0.65	0.3	1	4	952.23	151.88
24	298126	5049584	6	0.975	0.45	1	6	852.23	252.88
25	298077	5049498	4	0.65	0.3	1	4	752.23	156.85
26	298019	5049414	2	0.325	0.15	1	2	652.23	56.85
27	297964	5049333	4	0.65	0.3	1	4	752.23	156.85
28	297911	5049249	6	0.975	0.45	1	6	852.23	256.85
29	297855	5049160	6	0.975	0.45	1	6	952.23	266.42
30	297801	5049076	4	0.65	0.3	1	4	897.52	166.42
31	297749	5048990	2	0.325	0.15	1	2	797.52	66.42
32	297696	5048904	2	0.325	0.15	1	2	897.52	60.14
33	297637	5048818	2	0.325	0.15	1	2	997.52	60.51
34	297585	5048732	4	0.65	0.3	2	2	1097.52	91.77
35	297533	5048647	8	1.3	0.6	2	4	1197.52	191.77

36	297478	5048563	12	1.95	0.9	2	6	1297.52	291.77
37	297426	5048479	21	3.4125	1.575	3	7	1397.52	341.31
38	297370	5048394	15	2.4375	1.125	3	5	1497.52	241.31
39	297317	5048310	12	1.95	0.9	4	3	1597.52	141.31
40	297265	5048224	8	1.3	0.6	4	2	1697.52	41.31
41	297210	5048140	10	1.625	0.75	5	2	1794.13	57.37
42	297158	5048054	16	2.6	1.2	4	4	1694.13	157.37
43	297103	5047970	24	3.9	1.8	4	6	1594.13	257.37
44	297050	5047885	21	3.4125	1.575	3	7	1494.13	357.37
45	296994	5047802	18	2.925	1.35	3	6	1394.13	259.05
46	296941	5047716	8	1.3	0.6	2	4	1294.13	159.05
47	296890	5047631	4	0.65	0.3	2	2	1194.13	59.05
48	296838	5047543	8	1.3	0.6	2	4	1294.13	159.05
49	296783	5047459	6	0.975	0.45	3	2	1394.13	94.89
50	296728	5047374	6	0.975	0.45	3	2	1494.13	34.32
51	296675	5047288	12	1.95	0.9	4	3	1594.13	134.32
52	296619	5047201	8	1.3	0.6	4	2	1694.13	63.56
53	296571	5047113	10	1.625	0.75	5	2	1794.13	80.89
54	296513	5047032	20	3.25	1.5	5	4	1894.13	180.89
55	296463	5046947	36	5.85	2.7	6	6	1994.13	267.5
56	296410	5046861	24	3.9	1.8	6	4	2024.18	167.5
57	296353	5046777	10	1.625	0.75	5	2	1924.18	67.5
58	296289	5046700	10	1.625	0.75	5	2	1824.18	83.42
59	296217	5046632	16	2.6	1.2	4	4	1724.18	183.42
60	296140	5046565	24	3.9	1.8	4	6	1624.18	283.42
61	296052	5046517	15	2.4375	1.125	3	5	1524.18	223.37
62	295970	5046460	9	1.4625	0.675	3	3	1424.18	123.37
63	295881	5046414	2	0.325	0.15	2	1	1324.18	23.37
64	295795	5046362	4	0.65	0.3	2	2	1224.18	68.04
65	295707	5046315	2	0.325	0.15	2	1	1212.71	31.96
66	295621	5046266	6	0.975	0.45	2	3	1312.71	131.96
67	295534	5046214	15	2.4375	1.125	3	5	1412.71	231.96
68	295446	5046164	18	2.925	1.35	3	6	1512.71	282.2
69	295360	5046114	16	2.6	1.2	4	4	1612.71	182.2
70	295275	5046062	8	1.3	0.6	4	2	1712.71	82.2
71	295192	5046006	5	0.8125	0.375	5	1	1812.71	17.8
72	295111	5045947	15	2.4375	1.125	5	3	1912.71	117.8
73	295030	5045886	30	4.875	2.25	6	5	2012.71	217.8
74	294952	5045822	42	6.825	3.15	6	7	2112.71	317.8
75	294874	5045761	56	9.1	4.2	7	8	2212.71	417.8
76	294798	5045696	56	9.1	4.2	7	8	2312.71	368.72
77	294712	5045644	48	7.8	3.6	8	6	2373.43	268.72
78	294618	5045608	28	4.55	2.1	7	4	2273.43	168.72

79	294522	5045579	14	2.275	1.05	7	2	2173.43	68.72
80	294421	5045562	12	1.95	0.9	6	2	2073.43	43.37
81	294332	5045517	18	2.925	1.35	6	3	1973.43	143.37
82	294245	5045464	25	4.0625	1.875	5	5	1873.43	243.37
83	294173	5045393	35	5.6875	2.625	5	7	1773.43	343.37
84	294118	5045310	28	4.55	2.1	4	7	1673.43	336.69
85	294064	5045226	20	3.25	1.5	4	5	1573.43	236.69
86	294013	5045140	9	1.4625	0.675	3	3	1473.43	136.69
87	293960	5045053	6	0.975	0.45	3	2	1373.43	36.69
88	293906	5044969	9	1.4625	0.675	3	3	1473.43	136.69
89	293855	5044883	20	3.25	1.5	4	5	1573.43	236.69
90	293811	5044793	28	4.55	2.1	4	7	1673.43	336.69
91	293769	5044702	40	6.5	3	5	8	1773.43	436.69
92	293730	5044610	50	8.125	3.75	5	10	1873.43	536.69
93	293687	5044519	60	9.75	4.5	6	10	1973.43	512.58
94	293647	5044427	48	7.8	3.6	6	8	2073.43	412.58
95	293605	5044336	42	6.825	3.15	6	7	2060.3	312.58
96	293561	5044247	30	4.875	2.25	6	5	1960.3	212.58
97	293521	5044155	15	2.4375	1.125	5	3	1860.3	112.58
98	293480	5044062	4	0.65	0.3	4	1	1760.3	12.58
99	293437	5043971	8	1.3	0.6	4	2	1660.3	46.97
100	293397	5043879	8	1.3	0.6	4	2	1661.29	53.1
101	293353	5043788	8	1.3	0.6	4	2	1761.29	69.73
102	293308	5043698	10	1.625	0.75	5	2	1861.29	86.93
103	293267	5043607	24	3.9	1.8	6	4	1961.29	186.93
104	293224	5043512	36	5.85	2.7	6	6	2061.29	286.74
105	293180	5043422	28	4.55	2.1	7	4	2161.29	186.74
106	293135	5043332	14	2.275	1.05	7	2	2261.29	86.74
107	293077	5043249	16	2.6	1.2	8	2	2361.29	38.89
108	293027	5043162	24	3.9	1.8	8	3	2461.29	138.89
109	292992	5043068	32	5.2	2.4	8	4	2561.29	185.3
110	292968	5042969	18	2.925	1.35	9	2	2661.29	85.3
111	292940	5042873	18	2.925	1.35	9	2	2761.29	38.37
112	292914	5042774	27	4.3875	2.025	9	3	2861.29	138.37
113	292880	5042678	40	6.5	3	10	4	2961.29	158.04
114	292850	5042585	18	2.925	1.35	9	2	2868.29	58.04
115	292807	5042493	20	3.25	1.5	10	2	2905.66	83.21
116	292767	5042400	30	4.875	2.25	10	3	3005.66	125
117	292725	5042308	10	1.625	0.75	10	1	3105.66	25
118	292687	5042215	20	3.25	1.5	10	2	3205.66	76.54
119	292642	5042126	40	6.5	3	10	4	3305.66	176.54
120	292601	5042035	60	9.75	4.5	10	6	3405.66	276.54
121	292559	5041943	80	13	6	10	8	3505.66	376.54

122	292511	5041852	100	16.25	7.5	10	10	3605.66	476.54
123	292474	5041762	100	16.25	7.5	10	10	3705.66	521.54
124	292426	5041671	80	13	6	10	8	3805.66	421.54
125	292383	5041580	70	11.375	5.25	10	7	3796.41	321.54
126	292346	5041487	50	8.125	3.75	10	5	3696.41	221.54
127	292305	5041396	30	4.875	2.25	10	3	3596.41	121.54
128	292262	5041303	10	1.625	0.75	10	1	3496.41	21.54
129	292223	5041211	20	3.25	1.5	10	2	3396.41	71.34
130	292181	5041120	40	6.5	3	10	4	3296.41	171.34
131	292140	5041029	60	9.75	4.5	10	6	3196.41	271.34
132	292102	5040936	80	13	6	10	8	3096.41	371.34
133	292061	5040845	70	11.375	5.25	10	7	2996.41	356.78
134	292020	5040753	54	8.775	4.05	9	6	2896.41	256.78
135	291976	5040662	36	5.85	2.7	9	4	2796.41	156.78
136	291932	5040571	18	2.925	1.35	9	2	2696.41	56.78